The DOI for this manuscript is doi: 10.1175/JAS-D-15-0325.1

Ramirez, E., P. Dias, and C. Raupp, 2017: Multiscale atmosphere-ocean interactions and the low frequency variability in the equatorial region. J. Atmos. Sci. doi:10.1175/JAS-D-15-0325.1, in press.

Multiscale atmosphere-ocean interactions and the low frequency variability in the equatorial region

Enver Ramirez* and Pedro L da Silva Dias† and Carlos F. M. Raupp‡

**Corresponding author address:* Enver Ramirez, CPTEC/INPE, Rod. Presidente Dutra, km 40., Cachoeira Paulista, São Paulo cep 12630-000.
E-mail: enver.ramirez@gmail.com
†IAG/USP, Rua do Matão, 1226, Butantã, São Paulo, cep 05508-090
‡IAG/USP, Rua do Matão, 1226, Butantã, São Paulo, cep 05508-090

ABSTRACT

In the present study a simplified multiscale atmosphere-ocean coupled model for the tropical interactions among synoptic, intraseasonal and interannual scales is developed. Two nonlinear equatorial β-plane shallow water equations are considered: one for the ocean and the other for the atmosphere. The nonlinear terms are: the intrinsic advective nonlinearity and the air-sea coupling fluxes. To mimic the main differences between the fast-atmosphere and the slow-ocean, suitable anisotropic multi space/time scalings are applied, yielding a balanced **S**ynoptic/**In**traseasonal/interannual-**E**l **N**iño (**SInEN**) regime. In this distinguished balanced regime, the synoptic is the fastest atmospheric time-scale, the intraseasonal is the intermediate air-sea coupling time-scale (common to both fluid flows) and El Niño refers to the slowest interannual ocean time-scale. The asymptotic SInEN equations reveal that the slow wave amplitude evolution depends on both types of nonlinearities. Analytic solutions of the reduced SInEN equations for a single atmosphere-ocean resonant triad illustrate the potential of the model to understand slow frequency variability in the tropics. The resonant nonlinear wind stress allows a mechanism for the synoptic scale atmospheric waves to force intraseasonal variability in the ocean. The intraseasonal ocean temperature anomaly coupled with the atmosphere through evaporation forces synoptic and intraseasonal atmospheric variability. The wave-convection coupling provides another source for higher order atmospheric variability. Nonlinear interactions of intraseasonal ocean perturbations may also force interannual oceanic variability. The constrains that determine the establishment of the atmosphere-ocean resonant coupling can be viewed as selection rules for the excitation of intraseasonal variability (MJO) or even slower interannual variability (El Niño).

1. Introduction

Although incoming solar radiation is the main external energy source for the planet, the terrestrial components (atmosphere, hydrosphere, biosphere and lithosphere) manage the energy input and define both the fast (weather-scale) and the slow (climate-scale) responses. Moreover, among the terrestrial components of the earth's system, the atmosphere and ocean (a sub-component of the hydrosphere) are the leading contributors (Gabites 1950; Fritz 1958). In the weather time-scale, there are outstanding variabilities from microscales to the intra-diurnal ($<$ 24 hrs), the mesoscale ($<$ 2 days) and at synoptic-scale (3 - 7 days). On the other hand, in the climate time-scale, vigorous spectral peaks are found in the intraseasonal (30-180 days), the inter-annual to El Niño (1.5 - 7 yrs) and the multidecadal ($>$ 10 yrs) time-scales.

Recent studies highlight that the persistent deficiency in modeling the slow climate response can be associated with a misrepresentation of the fast weather-scale variability (Innes 2002; Stevens and Bony 2013; Bony et al. 2015). There are also both observational (e.g. Johnson et al. 1999) and general circulation modeling (e.g. Inness et al. 2001) evidence of the modulation of weather scale phenomena by climate variability. In addition, due to the large gap between weather and climate time-scales, if the weather affects the climate, this connection ought to be through multiscale interaction mechanisms. Thus, a renewed interest in systematic methods to develop simplified multiscale atmospheric models for scale interactions can be noted (e.g. Majda and Klein 2003; Majda and Biello 2003; Biello and Majda 2005; Raupp and Silva Dias 2005, 2006, 2009, 2010). The scale interactions can be responsible for the connection between weather and climate responses and involve either upscale/downscale cascade fluxes (Torrence and Webster 1999; Biello and Majda 2005) or discrete wave interactions ((Raupp et al. 2008; Raupp and Silva Dias 2009, 2010)). In this context, the wave-wave interactions have been used to explain the generation of low frequency El Niño variability (e.g. Zebiak 1982; Zebiak and Cane 1987; Suarez and Schopf 1988; Battisti 1988) and the intraseasonal atmospheric variability (Raupp and Silva Dias 2009). In evoking nonlinear wave interaction theory, the rigorous constraints in discrete resonant wave-wave interactions have been used to explain how certain interactions are favored over others (Longuet-Higgins and Gill 1967; Domaracki and Loesch 1977; Majda et al. 1999; Holm and Lynch 2002; Raupp and Silva Dias 2009; Ripa 1982, 1983a,b).

The present study applies both multiscale methods and nonlinear wave interaction theory to formulate a model capable of describing scale interactions in a simplified coupled atmosphere-ocean system. The multiscale method adopted here is similar to that adopted by Majda and Klein (2003) for the atmosphere. Thus, our approach can be regarded as an extension of Majda and Klein's systematic multiscale method by including atmosphere-ocean coupling. Perhaps the most interesting feature of our approach is to retain the eigenvectors, atmospheric and oceanic wave modes as leading-order solutions, which in turn allows these modes to interact through the nonlinearity associated with atmosphere-ocean coupling fluxes.

Two types of nonlinearity are included: the intrinsic advective nonlinearity and the nonlinearity related to the physical processes. The latter includes both the coupling between large-scale waves and moist convection and the heat and momentum fluxes associated with the atmosphere-ocean coupling.

As the focus of the present paper is on the nonlinear interactions in the tropical region, we use the equatorial β-plane approximation. Once the model is scaled by suitable multi-time and multi-space scalings, a perturbation theory is adopted to further simplify the equations and to obtain a reduced and more tractable system describing the interactions involving synoptic, intraseasonal and interannual time-scales in the atmosphere-ocean coupled system.

The paper is organized as follows. In Section 2, the basic model equations are introduced and the outlines for the atmosphere-ocean coupling are provided. Suitable scalings to represent the SInEN regime are reviewed at the end of Section 2. In Section 3, parameterizations for the mass and momentum fluxes in the SInEN regime are discussed. In Section 4, the dynamics and physics are joined to formulate the SInEN model equations. The SInEN model evolves in three time-scales, from the equatorial synoptic up to the interannual through the air-sea coupling intraseasonal time-scale. The explicit equations for the scale interactions are obtained by asymptotic perturbation methods. In Section 5, analytic solutions of the reduced SInEN equations are illustrated for the case of a discrete resonant triad composed of an oceanic Kelvin mode interacting with an atmospheric Rossby mode and an atmospheric Kelvin mode through the parameterized atmosphere-ocean coupling fluxes. The analytic solutions demonstrate the potential of the physical parameterization terms ("physics") to yield slow frequency variability by making synoptic and intraseasonal scale waves to exchange energy in interannual time-scales. In addition, according to our theoretical model, other effects such as the wave-convection coupling in the atmosphere can also play an important role in the excitation of low frequency variability. In Section 5 we also analyze the spatial patterns of the involved waves and the resulting atmosphere-ocean coupling fluxes. Then we discuss a possible configuration, based on observed features of both the MJO an El Ninõ - Southern Oscillation (ENSO) phenomena, that makes the interaction associated with the selected triad plausible. In Section 6 we summarize the mechanisms that allow the multiscale atmosphere-ocean interactions in the novel nonlinear multiscale model developed here and discuss how this model can be used to explain the slow climate variability.

2. A basic coupled atmosphere-ocean model for the equatorial region

a. Model equations

A simplified coupled model to study the tropical multiscale air-sea wave interactions can be obtained by using two nonlinear shallow water models, one representing the ocean and the other the atmosphere. Although the advective nonlinearities are not directly responsible for the atmosphere-ocean energy exchange, they are preserved in (1). Thus the governing equations are given by:

$$\partial_t \mathbf{v}_a + \mathbf{v}_a \cdot \nabla \mathbf{v}_a + \beta y \mathbf{k} \times \mathbf{v}_a + g \nabla H_a = F_{v_a} \tag{1a}$$

$$\partial_t H_a + \mathbf{v}_a \cdot \nabla H_a + H_a \nabla \cdot \mathbf{v}_a = F_{H_a} \tag{1b}$$

$$\partial_t \mathbf{v}_o + \mathbf{v}_o \cdot \nabla \mathbf{v}_o + \beta y \mathbf{k} \times \mathbf{v}_o + g' \nabla H_o = F_{v_o} \tag{1c}$$

$$\partial_t H_o + \mathbf{v}_o \cdot \nabla H_o + H_o \nabla \cdot \mathbf{v}_o = F_{H_o} \tag{1d}$$

The subscript o (a) refers the ocean (atmosphere). The vector $(\mathbf{v}_o, H_o)$ represents the ocean state i.e., currents and thickness, while $(\mathbf{v}_a, gH_a)$ represents the horizontal wind and geopotential height, $g' = (\Delta\rho_o/\rho_o)g$ is the reduced gravity, and the equatorial Coriolis parameter is represented by the $\beta-$plane approximation (Gill 1982; Pedlosky 1987). The convention used in the atmosphere for its vertical structure is that the shallow water equations represent the lowest atmospheric portion of the first baroclinic mode (similar to Liu and Wang 2013). The source/sink terms are denoted by $F_{v_o}, F_{H_o}, F_{v_a}, F_{H_a}$ and the atmospheric height and ocean thickness are:

$$H_\nu = \bar{H}_\nu(1 + F_\nu h_\nu), \text{ with } \nu = \{a, o\} \tag{2}$$

where H_V is the dynamical height/thickness and $\bar{H}_V$ its time independent mean value. F_V is a non-dimensional measure of the amplitude perturbation and $F_V h_V$ is the height/thickness perturbation per unit of vertical length.

b. Scalings for the synoptic/intraseasonal/El Niño (SInEN) Regime

1) MULTI-SPACE HORIZONTAL SCALINGS

Since time and length scales in the atmosphere are different from those in the ocean, we use multiscale methods (Pedlosky 1987; Majda and Klein 2003; Biello and Majda 2005). For instance, in the tropical region, the zonal extension of the Pacific Ocean ($l_s = 15 \times 10^6$m) is a distinctive parameter. In the ocean, l_s allows for the delayed oscillator mechanism of the El Niño phenomenon (Philander 1999a), and, presumably, is the zonal extension of the Pacific Ocean one of the causes for El Niño to occur only in this tropical ocean. In the atmosphere, despite teleconnections, significant tropical spatial variability is at and within the l_s scale. Consequently, l_s is taken as the referential zonal planetary scale in our model. On the other hand, the effects of both rotation and latitudinal trapping for large-scale waves near the equator are measured through the equatorial Rossby deformation radius. Thus, two important spatial scales are introduced: the atmospheric (oceanic) Rossby deformation radius λ_a (λ_o), where $\lambda_a = \sqrt{C/\beta}$, with C referring to the atmospheric first baroclinic gravity wave speed, and $\lambda_o = \sqrt{C_o/\beta}$, with C_o representing the oceanic first baroclinic gravity wave speed. The parameters relating zonal and meridional length scales for each subsystem are given by the anisotropy parameters $\delta_a = \lambda_a/l_s$ and $\delta_o = \lambda_o/l_s$. Since $\lambda_o < \lambda_a < l_s$, the horizontal spatial scales are anisotropic (Schubert et al. 2009; Ramírez et al. 2011a,b) and, as $\lambda_o/\lambda_a = \lambda_a/l_s \approx \mathscr{O}[0.1]$, the balance relation $\delta_a = \delta_o^{1/2}$ is useful to describe the spatial scale separation.

2) VERTICAL FLUCTUATION SCALINGS

Consistent with previous models, the oceanic shallow water equations represent the active layer of the ocean, with mean thickness $\bar{H}_o = 150$m (e.g. Battisti 1988). In addition, observational records show that the fluctuations of the oceanic thermocline h_o are of about 30-50 m (Donguy and Meyers 1987), which therefore results in estimates for the oceanic non-dimensional height fluctuations $F_o = h_o/\bar{H}_o \approx \mathscr{O}[0.1]$. For the atmosphere, the allowed fluctuations in the equivalent height associated with the synoptic scale temperature fluctuations $\Delta\theta = 1.5 - 3.0$ K can be estimated through the hypsometric equation (c.f. Emanuel 1987; Klein and Majda 2006), resulting in a non-dimensional height fluctuation $F_a = h_a/\bar{H}_a \approx \mathscr{O}[0.1]$, which is consistent with the estimates adopted in the atmospheric asymptotic multiscale model of Klein and Majda (2006). Therefore, $F_\nu \approx \mathscr{O}[0.1]$, $\nu = \{o, a\}$, is suitable to represent both the height and thickness fluctuations in the atmosphere and ocean, respectively. Thus, hereafter we shall use $F = F_a = F_o = \mathscr{O}[0.1]$ to represent the vertical fluctuation in both the atmosphere and ocean.

3) MULTI-TIME SCALINGS

For multi-time scalings, the time-derivative is split into fast ($\tilde{\tau}$), intermediate (t) and slow changes (τ). The intermediate scale is the referential time-scale T_{ref}, and its neighboring scales are separated by the scale separation parameter ε:

$$\partial_t \to \varepsilon^{-1}\partial_{\tilde{\tau}} + \partial_t + \varepsilon\partial_\tau \tag{3}$$

For the SInEN regime considered here, T_{ref} is related to a measure of the air-sea coupling velocity U defined by:

$$U = \frac{1}{2}(v_{a_{\mathrm{ref}}} + C_o) \approx 4.0\,\mathrm{m/s}, \tag{4}$$

Reported values of $v_{a_{\text{ref}}}$, in the tropical troposphere, lie in the range of $1-9$ m/s (e.g. Reed and Recker 1971). Holton (2004), in his scale analysis of large scale motions in the tropics, adopted 10 m/s as the atmospheric horizontal velocity scale. Here, we have selected $v_{a_{\text{ref}}} = 5.5$ m/s (see Table 1). However, the same qualitative results are obtained if we select the large values for U used by Holton (2004). The oceanic gravity wave speed of the first baroclinic mode C_o lies in the range of 2.4 - 2.9 m/s (Ripa 1982; Battisti 1988), and here the reference value of $C_o = 2.5$ m/s is used. With these referential length and velocity scales, it follows that the referential time-scale T_{ref} is the intraseasonal time-scale $T_{\text{ref}} = T_{\text{Int}} = l_s/U = 43.4$ days. Therefore, for a time-scale separation $\varepsilon = \mathscr{O}[0.1]$, the neighboring time scales are the equatorial synoptic time scale $\varepsilon T_{\text{Int}} = 4.3$ days and the interannual time scale $\varepsilon^{-1} T_{\text{Int}} = 434$ days. Since $\mathscr{O}[U] = \mathscr{O}[C_o] = \mathscr{O}[v_{a_{\text{ref}}}]$, the same qualitative results can be obtained if we use either $v_{a_{\text{ref}}}$ or C_o instead of U. The model obtained with the above scalings spans from the synoptic to the interannual time-scales, with the intraseasonal scale as the coupling time-scale. It is noteworthy that, as $U < C$ (C: baroclinic gravity wave speed) in the atmosphere, l_s/U is related to the slow nonlinear advective time-scale. In contrast, for the ocean T_{Int} is the characteristic time-scale for the linear gravity wave propagation. This motivates the ansatz in (34) for the evolution of the model, which establishes that the atmosphere evolves using the fastest two time scales (synoptic and intraseasonal), and the ocean evolves using the slowest two time scales (intraseasonal and interannual).

c. Scaled Model for the SInEN Regime

Now, considering the above discussions, the following scalings are utilized:

Ocean scalings

$$
\begin{aligned}
t &= (l_s/U)t_*; \qquad & x &= l_s x_*; \qquad & y &= \lambda_o y_*; \\
h &= \bar{H}_o F h_*; \qquad & u &= U_o u_*; \qquad & v &= (\lambda_o U_o/l_s) v_*; \\
C_o &= \sqrt{g'\bar{H}_o} \approx U; \quad & \lambda_o &= \sqrt{U/\beta}; \qquad & \delta_o &= \lambda_o/l_s
\end{aligned} \tag{5a}
$$

Atmospheric scalings

$$
\begin{aligned}
t &= (l_s/U)t_*; \qquad & x &= l_s x_*; \qquad & y &= \lambda_a y_*; \\
h &= \bar{H}_a F h_*; \qquad & u &= U u_*; \qquad & v &= (\lambda_a U/l_s) v_*; \\
C &= \sqrt{g\bar{H}_a} \approx \varepsilon^{-1} U; \quad & \lambda_a &= \sqrt{C/\beta}; \qquad & \delta_a &= \lambda_a/l_s,
\end{aligned} \tag{5b}
$$

The referential intraseasonal time-scale $T_{\text{Int}} = l_s/U$ and the planetary zonal length scale l_s are common for both the atmosphere and ocean, while the other selected scalings are different for the two subsystems. Application of scalings (5) into (1) results in:

$$\partial_t u_a + \mathbf{v_a} \cdot \nabla u_a - \varepsilon^{-1} \delta_a \mathscr{F}_{r_a}^{-1} y v_a + \mathscr{F}_{r_a}^{-2} F \partial_x h_a = \tilde{F}^x_{\mathbf{v_a}}, \tag{6a}$$

$$\delta_a \partial_t v_a + \delta_a \mathbf{v_a} \cdot \nabla v_a + \varepsilon^{-1} \mathscr{F}_{r_a}^{-1} y u_a + \varepsilon^{-1} \mathscr{F}_{r_a}^{-2} F \partial_y h_a = \tilde{F}^y_{\mathbf{v_a}}, \tag{6b}$$

$$\partial_t h_a + \mathbf{v_a} \cdot \nabla h_a + F^{-1} \nabla \cdot \mathbf{v_a} + h_a \nabla \cdot \mathbf{v_a} = \tilde{F}_{H_a}; \tag{6c}$$

$$\partial_t u_o + \mathscr{F}_{r_o} \mathbf{v_o} \cdot \nabla u_o - y v_o + \frac{F}{\mathscr{F}_{r_o}} \partial_x h_o = \tilde{F}^x_{\mathbf{v_o}}, \tag{6d}$$

$$\delta_o \partial_t v_o + \delta_o \mathscr{F}_{r_o} \mathbf{v_o} \cdot \nabla v_o + \varepsilon^{-2} y u_o + \varepsilon^{-2} \frac{F}{\mathscr{F}_{r_o}} \partial_y h_o = \tilde{F}^y_{\mathbf{v_o}}, \tag{6e}$$

$$\partial_t h_o + \varepsilon \mathbf{v_o} \cdot \nabla h_o + \frac{\varepsilon}{F} \nabla \cdot \mathbf{v_o} + \varepsilon h_o \nabla \cdot \mathbf{v_o} = \tilde{F}_{H_o}; \tag{6f}$$

where the scaled forcing terms are given by:

$$\tilde{F}^x_{\mathbf{v_a}} = \frac{l_s}{U^2} F^x_{\mathbf{v_a}}, \; \tilde{F}^y_{\mathbf{v_a}} = \frac{l_s}{U^2} F^y_{\mathbf{v_a}}, \; \tilde{F}_{H_a} = \frac{l_s}{U \bar{H}_a F} F_{H_a}, \tag{7a}$$

$$\tilde{F}^x_{\mathbf{v_o}} = \frac{l_s}{\varepsilon U^2} F^x_{\mathbf{v_o}}, \; \tilde{F}^y_{\mathbf{v_o}} = \frac{l_s}{\varepsilon U^2} F^y_{\mathbf{v_o}}, \; \tilde{F}_{H_o} = \frac{l_s}{U \bar{H}_o F} F_{H_o}. \tag{7b}$$

In (6)-(7) above, δ_a is the atmospheric anisotropy parameter, $\mathscr{F}_{r_a} = U/C$ is the atmospheric Froude number and δ_o, $\mathscr{F}_{r_o} = U_o/C_o$ refer to their oceanic counterparts. Furthermore, with $\varepsilon = 0.1$, $l_s =$

15×10^6m, $U=4$ m/s, $\lambda_o=4.2\times10^5$m, $\bar{H}_o=150$m, $\bar{H}_a=250$m, $\beta=2.29\times10^{-11}\text{m}^{-1}\text{s}^{-1}$, $\lambda_a=15\times10^5$m; it follows that $\delta_a=\mathscr{O}[\varepsilon]$ and $\delta_o=\mathscr{O}[\varepsilon^2]$. Thus, as the oceanic Rossby deformation radius is one order of magnitude smaller than its atmospheric counterpart ($\delta_o<\delta_a$), the ocean is more zonally elongated than the atmosphere, and this is consistent with the observational estimates for the tropical latitudinal extension.

On the other hand, for typical values of the referential currents in the active ocean layer $U_o=0.3-0.5$ m/s $\approx\varepsilon U$, it follows that $\mathscr{F}_{r_o}=\mathscr{O}[\varepsilon]$. Thus, the scalings considered here yield the balance:

$$\delta_a=\delta_o^{1/2}=\mathscr{F}_{r_a}=\mathscr{F}_{r_o}=F_a=F_o=F=\varepsilon=0.1, \tag{8}$$

Therefore, following (Majda and Klein 2003; Biello and Majda 2005) ε can be used as the small parameter in our formal asymptotic development, that is, the reduced model for **S**ynoptic/**In**traseasonal/interannual-**E**l **N**iño interactions in the coupled atmosphere-ocean system is obtained for $\varepsilon\to0$, and the conservative choice $\varepsilon=\mathscr{O}[0.1]$ is physically reasonable. The balance relations in (8) are required for the singular terms in (6) to appear in a skew-symmetric form, which allows us to obtain energy estimates independent of ε and thus to guarantee the regularity of the solution (Majda 2002).

It is important to note that in the ocean the quasi-geostrophic balance regulates the dynamics at leading-order in ε, so that the nonlinearity is weak and the oceanic Strouhal number S_{tro} (Zdunkowski and Bott 1980) relating the advection to the local derivative is small. In contrast, in the atmosphere the nonlinear terms are of the same order as the local time derivatives and, therefore, the atmospheric Strouhal number $S_{tra}=\mathscr{O}[1]$. Consequently, if prognostic equations are considered, the advective nonlinearity is not negligible. In both the atmosphere and ocean, the meridional acceleration is weaker than its corresponding zonal acceleration, and the system is slightly dispersive, with the spectrum of normal modes being modified under such conditions. The linear and weakly nonlinear equatorial wave spectra undergoing a continuous transition between a fully non-dispersive regime to a dispersive regime, as a function of the anisotropy parameter, have been studied by Ramírez et al. (2011b).

In the atmosphere, for the case of a purely Rayleigh friction in the momentum forcing $\tilde{F}^x = ru_a$ with a particularly strong damping $r^{-1} = 2$ days, the Gill-type model is recovered. Thus, to leading-order in ε, the atmosphere is rapidly adjusted to the ocean. In such a case, the memory of the system is in the ocean, and the dynamical component of (6) is basically the same as that used by Battisti (1988); Philander (1999b). The advantage of our approach is that (6) allows for linear waves in both the atmosphere and ocean, along with nonlinear effects coupling these modes.

Moreover, for the atmosphere, the scalings (5) are consistent with those used by Biello and Majda (2005) to obtain the IPESD (Intraseasonal planetary equatorial synoptic dynamics) model. Likewise, the scalings for the ocean are consistent with those used by (Battisti 1988; Philander 1999b; Dijkstra 2000).

In the real atmosphere-ocean coupled system, there are indications that the Madden-Julian Oscillation (MJO) can trigger El Niño (McPhaden 1999). However, not all MJO events trigger an El Niño event, and, consequently, there might exist a nontrivial selection rule. As we shall see later, a possible selection rule that might lead the MJO to excite interannual El Niño variability refers to wave triad resonance associated with the mass and momentum forcings that couple atmosphere and ocean.

3. Physical parameterizations for the SInEN model

a. Physics of the coupling

According to Dijkstra (2000), the sea surface temperature anomalies (SSTA) force changes in the low level winds through pressure differences directly induced by the temperature gradients or through pressure gradients associated with sensible and latent heat fluxes controlled by the sea surface temperature (SST). As a result, the wind changes result in modifications of the wind stress, which induce changes in the currents and drive further changes in the sea surface temperature (SST) (see also Wang and Weisberg 1994; Philander 1999b). Thus, it is necessary to include an equation for the SST to close model (1). Other processes and some limitations of the parameterizations here used are discussed in Section 6.

b. Momentum flux

The low level surface winds impinge a stress $\vec{\tau}$ onto the surface that transfers momentum to the ocean. In principle, this flux is parameterized by the bulk formula (Krishnamurti et al. 1998; Rogers 1976). However, as the flux is transferred throughout the active water column, the stress is weighted by the factor $\rho_o\bar{H}_o$ (proportional to the depth of the layer). Thus,

$$F_{V_o} = \frac{\vec{\tau}}{\rho_o\bar{H}_o} = \frac{\rho_a C_d|\vec{\mathbf{v}}_a|\vec{\mathbf{v}}_a}{\rho_o\bar{H}_o}, \tag{9}$$

where ρ_a is the air density, C_d the drag coefficient for momentum and ρ_o the water density. Furthermore, we consider the case in which $\vec{\tau}$ is dominated by the zonal wind stress (Cane and Sarachik 1976; Dijkstra 2000). The elimination of the meridional wind stress is also consistent with the dominant geostrophic balance in the meridional momentum equation. Thus, $F^y_{V_o} = 0$, $F^x_{V_o} = (\rho_a C_d|u_a|u_a)/(\rho_o\bar{H}_o)$ and the dimensionless wind stress $\tilde{F}^x_{V_o} = (l_s/\varepsilon U)F^x_{V_o}$ used in the scaled model equations is given by:

$$\tilde{F}^x_{V_o} = C_{\text{Mflx}} u^2_{a*}, \tag{10}$$

where the coefficient for momentum exchange is given by:

$$C_{\text{Mflx}} = \frac{l_s}{\varepsilon U^2} \frac{\rho_a C_d U^2 \, \text{sign}(u_{a*})}{\rho_o \bar{H}_o}. \tag{11}$$

MOMENTUM FLUX STRENGTH

To access the order in ε at which the momentum forcing must contribute, we first estimate the strength of the momentum flux ($\|F^x_{V_o}\|$). Thus, using the values in Table 1, it follows that $\|F^x_{V_o}\| = \frac{\rho_a C_d U^2}{\rho_o \bar{H}_o} \approx 0.12 \times 10^{-6}$ m/s^2, and the non-dimensional scaled strength ($\|\tilde{F}^x_{V_o}\|$) is given by

$$\|\tilde{F}^x_{V_o}\| = \frac{l_s}{\varepsilon U^2} \|F^x_{V_o}\| \approx 1.21 = \mathscr{O}[\varepsilon^0]. \tag{12}$$

c. Mass flux

The mass flux F_{H_a} is set as the difference between evaporation E and deep convective precipitation P, that is,

$$F_{H_a} = E - P, \tag{13}$$

With the sign convention adopted in (13), it is assumed that evaporation supplies mass to the atmosphere, whereas precipitation removes mass from it. Although this assumption is adequate for the basin wide zonal scale considered, it can break down for smaller scales; for example when the effects of the water vapor on the density must be considered.

1) EVAPORATION

The moisture flux is given by the bulk formula, which reads $E = \rho_a C_q L_v |\mathbf{v_a}| (q_s - q_a)$, where ρ_a is the air density, C_q the drag coefficient for water vapor flux, L_v the latent heat of vaporization,

q_s and q_a are the saturation and anemometer level moisture, respectively. Analogous to the wind stress forcing we use $|\mathbf{v_a}| \approx |u_a|$. Thus,

$$E = \rho_a C_q L_v |u_a| (q_s - q_a). \tag{14}$$

As in Neelin and Zeng (2000), the anemometer level moisture q_a is split in two parts, namely: $q_a = q_r + \Delta q_r$, where q_r is a referential time/spatial independent moisture and Δq_r represents local departures from q_r. Although several processes can be accommodated in Δq_r, such as the mesoscale/synoptic scale structure and evolution, we will set $\Delta q_r = 0$. This shortcoming will somehow be fixed later as the synoptic scale mass flux Q_{synoptic} will emerge as necessary forcing in order to close the model equations and to excite the lowest order perturbations in the atmosphere. The saturation moisture q_s can be approximated by

$$q_s \approx \frac{e_s(T) R_d}{p R_v}, \tag{15}$$

where e_s is the saturation water vapor pressure, p is a referential pressure and $R_d/R_v = 0.622$. The temperature T is split into basic state temperature $\bar{T}$ and anomalous temperature T'. Then, by using the Clausius-Clapeyron equation $\frac{de_s}{dT} = \frac{L_v(T) e_s}{R_v T^2}$ and neglecting the temperature dependency of the latent heat of vaporization, we obtain

$$q_s(T') = \frac{\gamma^* R_d}{p_0 R_v} \big(1 + \frac{L_v T'}{R_v \bar{T}^2}\big) \tag{16}$$

where $\gamma^* = e_{s0} \exp\big(\frac{L_v}{R_v}(\frac{1}{T_0} - \frac{1}{\bar{T}})\big)$, $e_{s0} = 6.11$ mb, $T_0 = 273.0$ K and $p_0 = 1000$ hPa. Thus, the moisture flux as a function of T' and u_a is given by

$$E(T', u_a) = C_u |u_a| + C_T |u_a| T' \tag{17}$$

where C_u and C_T are non-dimensional coefficients for the linear and nonlinear components of the moisture flux

$$C_u = \frac{l_s}{U\bar{H}_a F}\,\rho_a C_q L_v U\,(\frac{\gamma^* R_d}{p_0 R_v} - [q_r]), \tag{18a}$$

$$C_T = \frac{l_s}{U\bar{H}_a F}\,\rho_a C_q L_v U\,(\frac{\gamma^* R_d}{p_0 R_v}\frac{L_v[T']}{R_v\bar{T}^2}). \tag{18b}$$

In the equations above, $[q_r]$ and $[T']$ represent the dimensional strength of moisture and sea surface temperature anomalies, respectively. Differently from Liu and Wang (2013), the expression for E contains a nonlinear term yielding a coupling between temperature and wind.

2) THERMODYNAMIC EQUATION

The approximate thermodynamic equation with dissipation rate r, radiative forcing S and horizontal and vertical advection is given by

$$\partial T'/\partial t = -\varepsilon\tilde{\mathbf{v}}_{\mathbf{o}}\cdot\nabla T' - w_o\partial T'/\partial z - rT' + S. \tag{19}$$

Simplified versions of (19) can be obtained, for the case of weak horizontal advection ($\varepsilon \to 0$) and no radiative forcing (i.e. $S = 0$). Moreover, the vertical advection depends on the vertical gradient associated with the difference between surface T' and the subsurface T_s temperature anomalies. Thus,

$$-w_o\frac{\partial T'}{\partial z} \approx -w_o\frac{T' - T_s}{\bar{H}_o} = -w_o\frac{T'}{\bar{H}_o} + K_T h_o \tag{20}$$

where K_T relates the subsurface temperature anomaly to the height perturbation h_o (Battisti 1988).

In addition, in the fast thermodynamic adjustment, $\partial T'/\partial t \to 0$, the sea surface temperature anomaly can also be related to the height perturbation through the following expression:

$$r^* T' = (r + \frac{w_o}{\bar{H}_o})T' = K_T h_o \tag{21}$$

where r^* is the dissipation rate modified by the vertical advection. With the aid of the thermodynamic equation (21), the moisture flux can be written as a function of the ocean height perturbation

$$E(h_o, u_a) = C_u|u_a| + C_h|u_a|h_o \tag{22}$$

where

$$C_h = \frac{l_s}{U\bar{H}_a F}\rho_a C_q L_v C\,(\frac{\gamma^* R_d}{p_0 R_v}\frac{L_v}{R_v\bar{T}^2}\frac{K_T[h_o]}{r^*}) \tag{23}$$

and C_h is related to C_T by

$$C_h = \frac{K_T[h_o]}{r^*[T']}C_T. \tag{24}$$

EVAPORATION STRENGTH

In order to access the evaporation strength, temperature fluctuations in the tropical atmosphere $\Delta\theta$ are used as proxy of the moisture fluctuations Δq_r in the same region. In this way, Δq_r is used to estimate the moisture flux. Following Majda and Shefter (2001b), the typical magnitude of temperature fluctuations in the tropical troposphere is given by $\Delta\theta = (\theta_0 - \bar{\theta})/\theta_0 \approx 0.1$ for a referential temperature $\theta_0 = 300$K. This estimate is roughly valid for specific moisture fluctuations

$$\Delta q_r \approx \frac{C_p}{L_v}\Delta\theta \approx 12 \text{ g/kg}. \tag{25}$$

Thus, the evaporation strength is given by $\|E\| = 2.29\times 10^5$ W/m^2, or in m/s

$$\|E\| = 4.9\times 10^3\, u_a\, \Delta q_r = 0.94\times 10^{-4} \text{ m/s} \tag{26}$$

The dimensionless evaporation strength using E in m/s results in

$$\|\tilde{F}^E_{H_a}\| = \frac{l_s}{U\bar{H}_a F}\|E\| \approx 1.4\varepsilon^{-1} = \mathscr{O}[\varepsilon^{-1}] \tag{27}$$

3) PRECIPITATION

Precipitation is parameterized by the low level moisture convergence due to anomalous winds according to

$$P = \lambda_p \int_0^{h_b} \mathscr{H}(-\nabla\cdot(q_v \mathbf{v}_a))dz \approx \lambda_p h_b \mathscr{H}(-\nabla\cdot(q_v \mathbf{v}_a)) \tag{28}$$

where λ_p is the precipitation efficiency, h_b is the boundary layer depth given by $h_b = \varepsilon \bar{H}_a$, q_v is the moisture field and $\mathscr{H}(x) = x$ for $x \geq 0$ and zero otherwise. If the moisture field q_v is approximated by the time/spatial independent referential moisture q_r, then P is given by:

$$P \approx C_{Pr} \mathscr{H}(-\nabla\cdot\vec{\mathbf{v}}_a) \tag{29}$$

where,

$$C_{Pr} = \frac{l_s}{U\bar{H}_a F}\frac{\lambda_p h_b q_r U}{l_c} \tag{30}$$

PRECIPITATION STRENGTH

In the tropics, several hierarchies of the organization of clouds and precipitation are found (Nakazawa 1988). In general, P is confined to a region whose length scale l_c is smaller than l_s, with l_c representing a measure of spatial organization of clouds and precipitation. In the upper limit, $l_c \approx l_s$, P represents planetary scale precipitation as in the Intertropical Convergence Zone (ITCZ) or the Madden-Julian oscillation (MJO) envelope (Nakazawa 1988). Smaller hierarchies of clouds lead to smaller values of l_c. Examples of these smaller hierarchies of cloud organization are the planetary scale organization by cloud clusters with $l_c \approx 100$ km, super-clusters of synoptic scale organization (SYSO) with $l_c = \varepsilon l_s \approx 1500$ km and mesoscale organization (MESO) with $l_c = \varepsilon l_s/\pi \approx 500$ km .

The dimensionless precipitation strength for a precipitation efficiency parameter $\lambda_p = 0.9$ (see ε_p in Majda and Shefter 2001b) and a planetary scale precipitation with $l_c = l_s$ is then estimated as follows:

$$\|\tilde{F}^{P}_{H_a}\| = \frac{l_s}{U\bar{H}_a F}\frac{\lambda_p h_b q_r U}{l_c} \approx 1.1\varepsilon^{-1} = \mathscr{O}[\varepsilon^{-1}] \tag{31}$$

Furthermore, for heating regions associated with the MJO $\tilde{F}^{P}_{H_a} \approx 1.7\varepsilon^{-1}$. In addition, for synoptic scale heating we have $\tilde{F}^{P}_{H_a} \approx 11.0\varepsilon^{-1}$. These numbers agree quite well with other estimates (Majda and Shefter 2001b,a; Yano et al. 1995).

MASS FLUX STRENGTH

The mass flux ($\tilde{F}_{H_a}$) is given by the balance between E and P and its strength is determined by

$$\tilde{F}_{H_a} = \frac{l_s}{U\bar{H}_a F}(F^{E}_{H_a} - F^{P}_{H_a}) \tag{32}$$

For the hierarchies of clouds and precipitation discussed above, we have:

$$\tilde{F}_{H_a} = \begin{cases} +3.0\varepsilon^{0} & : l_c = l_s \,(\text{ITCZ}) \\ -3.0\varepsilon^{0} & : l_c \approx l_s \,(\text{MJO}) \\ -9.6\varepsilon^{-1} & : l_c = \varepsilon l_s \,(\text{SYSO}) \end{cases} \tag{33}$$

Considering the whole budget in (33) implies that in the tropical region precipitation is larger than evaporation ($\tilde{F}_{H_a}(ITCZ) + \tilde{F}_{H_a}(MJO) + \tilde{F}_{H_a}(SYSO) < 0$). However, in the planetary ITCZ-like organization, as $\tilde{F}_{H_a}$ is positive, the atmosphere has a net gain of mass (evaporation stronger than precipitation). In contrast, for smaller organization systems, such as in the planetary MJO-like or in the SYSO-like structures, it follows that precipitation is stronger than evaporation, resulting in a negative mass source and a net mass loss. Therefore, it appears that the scale of moisture convergence l_c can be used as a bifurcation parameter.

4. Multiscale SInEN model

Let us assume now that each component of the system has a solution composed of leading order $(\vec{v}^{(0)}_{\nu}, h^{(0)}_{\nu})$ and higher order $(\vec{v}^{(1)}_{\nu}, h^{(1)}_{\nu})$ perturbations, with $\nu = (a,o)$ indicating the atmosphere and the ocean, respectively. We should remember that in our scaled model the ocean evolves in the slowest two time-scales (t, τ), whereas the atmosphere evolves in the fastest two time-scales $(\tilde{\tau}, t)$. Then the following ansatz is assumed:

$$\vec{\mathbf{v}}_a(\tilde{\tau},t,\mathbf{x}) = \vec{\mathbf{v}}_a^{(0)}(\tilde{\tau},t,\mathbf{x}) + \varepsilon \vec{\mathbf{v}}_a^{(1)}(\tilde{\tau},\mathbf{x}); \tag{34a}$$

$$h_a(\tilde{\tau},t,\mathbf{x}) = h_a^{(0)}(\tilde{\tau},t,\mathbf{x}) + \varepsilon h_a^{(1)}(\tilde{\tau},\mathbf{x}) \tag{34b}$$

$$\vec{\mathbf{v}}_o(t,\tau,\mathbf{x}) = \vec{\mathbf{v}}_o^{(0)}(t,\tau,\mathbf{x}) + \varepsilon \vec{\mathbf{v}}_o^{(1)}(t,\mathbf{x}); \tag{34c}$$

$$h_o(t,\tau,\mathbf{x}) = h_o^{(0)}(t,\tau,\mathbf{x}) + \varepsilon h_o^{(1)}(t,\mathbf{x}). \tag{34d}$$

with $\tilde{\tau}, t$ and τ indicating synoptic, intraseasonal and interannual time-scales, respectively. To ensure the uniform validity of the expansion (34), the solvability condition imposes that: *If there is any growth of the highest order terms, the growth must be slower than the linear growth (Kevorkian and Cole 1986)*, that is:

$$\lim_{\varepsilon \to 0} \left(\frac{\vec{\mathbf{v}}_\nu^{(1)}(\varepsilon^{-1},\mathbf{x})}{|\varepsilon^{-1}|+1} \right) = 0 \tag{35a}$$

$$\lim_{\varepsilon \to 0} \left(\frac{h_\nu^{(1)}(\varepsilon^{-1},\mathbf{x})}{|\varepsilon^{-1}|+1} \right) = 0 \tag{35b}$$

Physically, (35) means that even after a long period $\mathscr{O}[\varepsilon^{-1}]$ the $(\vec{v}_\nu^{(1)}, h_\nu^{(1)})$ perturbations cannot overcome the leading order $(\vec{v}_\nu^{(0)}, h_\nu^{(0)})$ ones. In addition, consistently with the strength estimates the source terms can be expanded as:

$$F_{H_a} = \varepsilon^{-1} F_{H_a}^{(-1)} + F_{H_a}^{(0)} + \varepsilon F_{H_a}^{(1)}, \tag{36a}$$

$$F_{V_o} = F_{V_o}^{(0)} + \varepsilon F_{V_o}^{(1)}. \tag{36b}$$

with the oceanic momentum flux given by the wind stress parameterization

$$\left(\ \tilde{F}_{V_o}^{x(0)},\ \tilde{F}_{V_o}^{y(0)},\ \tilde{F}_{H_o}^{(0)}\ \right)^T = \left(\ C_{\text{Mflx}} u_a^{(0)^2},\ 0,\ 0\ \right)^T; \tag{37a}$$

$$\left(\ \tilde{F}_{V_o}^{x(1)}, \tilde{F}_{V_o}^{y(1)}, \tilde{F}_{H_o}^{(1)}\ \right)^T = \left(\ 2C_{\text{Mflx}} u_a^{(0)} u_a^{(1)}, 0, 0\ \right)^T; \tag{37b}$$

and the atmospheric heat flux given by:

$$\left(\ \tilde{F}_{V_a}^{x(-1)}, \tilde{F}_{V_a}^{y(-2)}, \tilde{F}_{H_a}^{(-1)}\ \right)^T = \left(\ 0, 0, Q_{\text{synoptic}}\ \right)^T; \tag{37c}$$

$$\left(\ \tilde{F}_{V_a}^{x(0)}, \tilde{F}_{V_a}^{y(-1)}, \tilde{F}_{H_a}^{(0)}\ \right)^T = \left(\ 0, 0, C_u u_a^{(0)} + C_h u_a^{(0)} h_o^{(0)} - C_{Pr} \mathscr{H}(-\nabla \cdot \vec{\mathbf{v}}_a^{(0)})\ \right)^T; \tag{37d}$$

$$\left(\ \tilde{F}_{V_a}^{x(1)}, \tilde{F}_{V_a}^{y(0)}, \tilde{F}_{H_a}^{(1)}\ \right)^T = \left(\ 0, 0, C_u u_a^{(1)} + C_h (u_a^{(1)} h_o^{(0)} + u_a^{(0)} h_o^{(1)}) - C_{Pr} \mathscr{H}(-\nabla \cdot \vec{\mathbf{v}}_a^{(1)})\ \right)^T. \tag{37e}$$

Once the leading order atmospheric mass flux Q_{synoptic} is specified (recall that it is a free parameter of the model), it drives the $(\vec{v}_a^{(0)}, h_a^{(0)})$ perturbations, and, in turn, a combination of the resulting perturbations constitutes either the atmospheric mass forcing for higher order disturbances $(\vec{v}_a^{(1)}, h_a^{(1)})$ or the momentum forcing for leading-order perturbations in the ocean $(\vec{v}_o^{(0)}, h_o^{(0)})$. The evaporation contributes with both linear and nonlinear terms, and precipitation was parameterized in terms of linear moisture convergence. In the ocean, the in-homogeneous term for $(\vec{v}_o^{(0)}, h_o^{(0)})$ is due to nonlinear combination of $(\vec{v}_a^{(0)}, h_a^{(0)})$ perturbations, whereas the forcing of $(\vec{v}_o^{(1)}, h_o^{(1)})$ presents a mixed $\mathscr{O}[\varepsilon^0]$-$\mathscr{O}[\varepsilon^1]$ term. Mixed terms also appear in the atmosphere, but only as a forcing for higher order terms that are not included in the present study. The physics introduces nonlinear terms related to the mass and momentum fluxes, and the nonlinear mass flux is related to the evaporative heat flux. Finally, inserting the ansatz (34) into the SInEN model equations yields:

Three time scale model for the synoptic/intraseasonal/El Niño (SInEN) regime

$$\partial_{\tilde{\tau}} u_a^{(0)} - y v_a^{(0)} + \partial_x h_a^{(0)} = \tilde{F}_{V_a}^{x\,(-1)}; \qquad (:\varepsilon^{-1}) \tag{38a}$$

$$y u_a^{(0)} + \partial_y h_a^{(0)} = \tilde{F}_{V_a}^{y\,(-2)}; \qquad (:\varepsilon^{-2}) \tag{38b}$$

$$\partial_{\tilde{\tau}} h_a^{(0)} + \nabla \cdot \mathbf{V}_a^{(0)} = \tilde{F}_{H_a}^{(-1)}; \qquad (:\varepsilon^{-1}) \tag{38c}$$

363

$$\partial_{\tilde{\tau}} u_a^{(1)} - y v_a^{(1)} + \partial_x h_a^{(1)} = \tilde{F}_{V_a}^{x\,(0)} - (\partial_t u_a^{(0)} + \mathbf{V}_a^{(0)} \cdot \nabla u_a^{(0)}); \qquad (:\varepsilon^{0}) \tag{38d}$$

$$y u_a^{(1)} + \partial_y h_a^{(1)} = \tilde{F}_{V_a}^{y\,(-1)}; \qquad (:\varepsilon^{-1}) \tag{38e}$$

$$\partial_{\tilde{\tau}} h_a^{(1)} + \nabla \cdot \mathbf{V}_a^{(1)} = \tilde{F}_{H_a}^{(0)} - (\partial_t h_a^{(0)} + \mathbf{V}_a^{(0)} \cdot \nabla h_a^{(0)} + h_a^{(0)} \nabla \cdot \mathbf{V}_a^{(0)}); \qquad (:\varepsilon^{0}) \tag{38f}$$

364

$$\partial_t u_o^{(0)} - y v_o^{(0)} + \partial_x h_o^{(0)} = \tilde{F}_{V_o}^{x\,(0)}; \qquad (:\varepsilon^{0}) \tag{38g}$$

$$y u_o^{(0)} + \partial_y h_o^{(0)} = \tilde{F}_{V_o}^{y\,(0)}; \qquad (:\varepsilon^{-3}) \tag{38h}$$

$$\partial_t h_o^{(0)} + \nabla \cdot \mathbf{V}_o^{(0)} = \tilde{F}_{H_o}^{(0)}; \qquad (:\varepsilon^{0}) \tag{38i}$$

365

$$\partial_t u_o^{(1)} - y v_o^{(1)} + \partial_x h_o^{(1)} = \tilde{F}_{V_o}^{x\,(1)} - (\partial_\tau u_o^{(0)} + \mathbf{V}_o^{(0)} \cdot \nabla u_o^{(0)}); \qquad (:\varepsilon^{1}) \tag{38j}$$

$$y u_o^{(1)} + \partial_y h_o^{(1)} = \tilde{F}_{V_o}^{y\,(1)}; \qquad (:\varepsilon^{-2}) \tag{38k}$$

$$\partial_t h_o^{(1)} + \nabla \cdot \mathbf{V}_o^{(1)} = \tilde{F}_{H_o}^{(1)} - (\partial_\tau h_o^{(0)} + \mathbf{V}_o^{(0)} \cdot \nabla h_o^{(0)} + h_o^{(0)} \nabla \cdot \mathbf{V}_o^{(0)}); \qquad (:\varepsilon^{1}) \tag{38l}$$

The ε powers between brackets in the right of their correspondent equations (38) indicate the order in which the equations are balanced.

The leading order perturbations of each subsystem are governed by the so-called linear equatorial long-wave equations, whose eigenvectors are the anisotropic non-dispersive Kelvin and Rossby waves (e.g. Gill 1980; Schubert et al. 2009; Ramírez et al. 2011b). Consequently, the solvability condition (35) applied in (38) implies that the source terms for the $(\vec{v}_a^{(1)}, h_a^{(1)})$ and $(\vec{v}_o^{(1)}, h_o^{(1)})$ perturbations must be non-resonant with the linear operator. Since the linear operator describes the anisotropic Rossby and Kelvin waves, the elimination of resonances is achieved by projecting the first order equations onto the Kelvin and Rossby wave eigenvectors, in their respective traveling reference frames (see, for instance, Boyd 1980; Majda and Biello 2003). This projection results in the slow evolution equations of the amplitudes of Kelvin and Rossby wave packets of both the atmosphere and ocean. These Rossby and Kelvin wave packets undergo their own self mode interactions due to the intrinsic advective nonlinearity of each subsystem (compare Gill 1980 and Gill and Phlips 1986). In addition, the parameterized mass and momentum fluxes coupling the atmosphere and ocean can yield interactions between atmospheric and oceanic wave packets through resonant triads of specific Fourier modes. This latter feature of the multiscale SInEN model is illustrated in the next section.

5. Integration of the multiscale SInEN model: the case of a single resonant triad interaction

As discussed above, in the multiscale SInEN model (38) wave modes are allowed in both the atmosphere and ocean sub-systems and the leading order solution corresponds to the anisotropic non-dispersive Kelvin and long Rossby waves. Furthermore, nonlinear mode interactions are due to either the advective nonlinearity or the parameterized mass and momentum forcings. The former allows for interactions of waves that belong to the same sub-system, whereas the latter allows for across sub-system mode interactions. In this section, we deal with the nonlinear wave interaction of atmospheric and oceanic waves through wind stress and evaporation and how these interactions can connect atmosphere and ocean from synoptic to interannual time-scales through intraseasonal time-scale.

a. Solvability condition and resonant triad equations

The source terms for the $\mathscr{O}[\varepsilon]$ perturbations in both the atmosphere (38d-38f) and ocean (38j-38l) have the form of a forced Burger equation, which is a model for the nonlinear interaction of non-dispersive wave packets (e.g. Boyd 1980; Menzaque et al. 2001). However, as our focus is on interactions involving waves of different media, we neglect the advective terms and restrict our analysis to the discrete wave mode interactions produced by the physical parameterizations. The motivation for this simplification comes from Fig. 2, where a representative example of atmosphere-ocean resonant triad is depicted. The triad is composed of atmospheric Kelvin and Rossby waves along with an oceanic Kelvin wave represented by (ω_1, k_1); (ω_2, k_2) and (ω_3, k_3), respectively. The resonance condition for this discrete triad interaction is given by:

$$\omega_1 = \omega_2 + \omega_3, \tag{39a}$$

$$k_1 = k_2 + k_3. \tag{39b}$$

Therefore, in order to study the dynamics of this resonant triad, we consider the following ansatz for the leading-order solution of SInEN model:

$$\begin{pmatrix} u_a \\ v_a \\ h_a \end{pmatrix} = Z_1(t) \begin{pmatrix} \hat{u}_1(\varepsilon y) \\ \hat{v}_1(\varepsilon y) \\ \hat{h}_1(\varepsilon y) \end{pmatrix} \mathrm{e}^{i(k_1 x - \omega_1 \tilde{\tau})} + Z_2(t) \begin{pmatrix} \hat{u}_2(\varepsilon y) \\ \hat{v}_2(\varepsilon y) \\ \hat{h}_2(\varepsilon y) \end{pmatrix} \mathrm{e}^{i(k_2 x - \omega_2 \tilde{\tau})} + \text{C.C.} \tag{40a}$$

$$\begin{pmatrix} u_o \\ v_o \\ h_o \end{pmatrix} = Z_3(\tau) \begin{pmatrix} \hat{u}_3(y) \\ \hat{v}_3(y) \\ \hat{h}_3(y) \end{pmatrix} \mathrm{e}^{i(k_3 x - \omega_3 t)} + \text{C.C.}. \tag{40b}$$

In (40), the meridional structure functions $(\hat{u}_j, \hat{v}_j, \hat{h}_j,\ j = \{1,2,3\})$ are given by

$$\begin{pmatrix}\hat{u}_1\\ \hat{v}_1\\ \hat{h}_1\end{pmatrix} = \frac{1}{\sqrt{2\sqrt{\pi}}}\begin{pmatrix}1\\0\\1\end{pmatrix}\mathrm{e}^{-\varepsilon^2 y^2/2}; \begin{pmatrix}\hat{u}_3\\ \hat{v}_3\\ \hat{h}_3\end{pmatrix} = \frac{1}{\sqrt{2\sqrt{\pi}}}\begin{pmatrix}1\\0\\1\end{pmatrix}\mathrm{e}^{-y^2/2} \tag{41a}$$

$$\begin{pmatrix}\hat{u}_2\\ \hat{v}_2\\ \hat{h}_2\end{pmatrix} = \frac{1}{D}\begin{pmatrix} i[-(\omega_2+k_2)\psi_2(\varepsilon y)-(\omega_2-k_2)\sqrt{\frac{1}{2}}\psi_0(\varepsilon y)]\\ (\omega_2^2-k_2^2)\psi_1(\varepsilon y)\\ i[(\omega_2+k_2)\psi_2(\varepsilon y)-(\omega_2-k_2)\sqrt{\frac{1}{2}}\psi_0(\varepsilon y)]\end{pmatrix} \tag{41b}$$

where $D = [(\omega_2-k_2)^2+2(\omega_2+k_2)^2+(\omega_2^2-k_2^2)^2]$ and $\psi_j(y)$ are the Hermite functions. The weaker meridional confinement near the equator of the atmospheric waves is represented by $Y = \varepsilon y$ in the argument of the Hermite functions. Therefore, substituting the ansatz (40) in (38) it follows that the leading-order $\mathscr{O}[1]$ equations are satisfied automatically, since the ansatz is a combination of three linearly independent solutions of the $\mathscr{O}[1]$ problem. Consequently, by requiring orthogonality between the in-homogeneous terms in the $\mathscr{O}[\varepsilon]$ equations and the linear operator to eliminate the secular terms yields:

$$\frac{d}{dt}Z_1 = L_1 Z_1 + N_1^{2,3} Z_2 Z_3 \tag{42a}$$

$$\frac{d}{dt}Z_2 = L_2 Z_2 + N_2^{3,1} Z_3^* Z_1 \tag{42b}$$

$$\frac{d}{dt}Z_3 = L_3 Z_3 + N_3^{1,2} Z_1 Z_2^* \tag{42c}$$

where the linear coefficients L_1, L_2 and L_3 are given by

$$L_1 \equiv [C_u\langle\hat{u}_1|\hat{h}_1\rangle + i\omega_1 C_{\mathrm{Pr}}\langle\hat{h}_1|\hat{h}_1\rangle] \tag{43a}$$

$$L_2 \equiv [C_u\langle\hat{u}_2|\hat{h}_2\rangle + i\omega_2 C_{\mathrm{Pr}}\langle\hat{h}_2|\hat{h}_2\rangle] \tag{43b}$$

$$L_3 \equiv 0 \tag{43c}$$

and the nonlinear interaction coefficients $N_1^{2,3}, N_2^{3,1}, N_3^{1,2}$ are

$$N_1^{2,3} \equiv C_h \left\langle \hat{u}_2 \hat{h}_3 | \hat{h}_1 \right\rangle \tag{44a}$$

$$N_2^{3,1} \equiv C_h \left\langle \hat{u}_1 \hat{h}_3 | \hat{h}_2 \right\rangle \tag{44b}$$

$$N_3^{1,2} \equiv 2\varepsilon C_{\mathrm{Mflx}} \left\langle \hat{u}_1 \hat{u}_2 | \hat{u}_3 \right\rangle \tag{44c}$$

The multiplicative factor ε in the nonlinear interaction coefficient of the oceanic mode reflects the slower time-scale associated to the oceanic mode amplitude compared to the atmospheric waves. The inner product $\langle \, | \, \rangle$ is defined by

$$\langle \vec{f} | \vec{g} \rangle = \lim_{T\to\infty} \frac{1}{T} \int_0^T \lim_{L\to\infty} \frac{1}{L} \int_0^L \int_{-\infty}^{\infty} (\vec{f}^{\dagger} \cdot \vec{g}) dy dx dt \tag{45}$$

The time and zonal dependency can be evaluated using

$$\lim_{S\to\infty} \frac{1}{S} \int_0^S \mathrm{e}^{i\Delta s} ds = \begin{cases} 1 \text{ for } \Delta = 0, \\ \\ 0 \text{ for } \Delta \neq 0. \end{cases} \tag{46}$$

By considering the transformation $Z_j = \hat{Z}_j e^{L_j t}, j = \{1,2,3\}$, and omitting the hats for simplicity, the equations (42) can be re-written to focus on the nonlinear terms

$$\frac{d}{dt} Z_1 = N_1^{2,3} Z_2 Z_3 \tag{47a}$$

$$\frac{d}{dt} Z_2 = N_2^{3,1} Z_1 Z_3^* \tag{47b}$$

$$\frac{d}{dt} Z_3 = N_3^{1,2} Z_1 Z_2^* \tag{47c}$$

Furthermore, evaluating the nonlinear coupling coefficients we have:

$$\left\langle \hat{u}_2 \hat{h}_3 | \hat{h}_1 \right\rangle = \left(+\Gamma I_{200}^{\varepsilon 1 \varepsilon} + \Lambda I_{000}^{\varepsilon 1 \varepsilon} \right) \tag{48a}$$

$$\left\langle \hat{u}_1 \hat{h}_3 | \hat{h}_2 \right\rangle = \left(-\Gamma I_{200}^{\varepsilon 1 \varepsilon} + \Lambda I_{000}^{\varepsilon 1 \varepsilon} \right) \tag{48b}$$

$$\left\langle \hat{u}_1 \hat{u}_2 | \hat{u}_3 \right\rangle = \left(+\Gamma I_{200}^{\varepsilon 1 \varepsilon} + \Lambda I_{000}^{\varepsilon 1 \varepsilon} \right) \tag{48c}$$

where

$$\Gamma = \frac{-i(\omega_2 + k_2)}{D} \tag{49a}$$

$$\Lambda = \frac{-i(\omega_2 - k_2)}{D} \tag{49b}$$

and

$$I_{000}^{\varepsilon 1 \varepsilon} \equiv \int_{-\infty}^{\infty} \psi_0(\varepsilon y)\psi_0(y)\psi_0(\varepsilon y)dy = \int_{-\infty}^{\infty} \frac{1}{\pi^{\frac{3}{4}}} \mathrm{e}^{-y^2(\varepsilon^2+\frac{1}{2})} dy = \frac{1}{\pi^{\frac{1}{4}}} \sqrt{\frac{1}{\varepsilon^2 + \frac{1}{2}}} \tag{50a}$$

$$I_{200}^{\varepsilon 1 \varepsilon} \equiv \int_{-\infty}^{\infty} \psi_2(\varepsilon y)\psi_0(y)\psi_0(\varepsilon y)dy = \int_{-\infty}^{\infty} \frac{2\varepsilon^2 y^2 - 1}{\sqrt{2}\pi^{\frac{3}{4}}} \mathrm{e}^{-y^2(\varepsilon^2+\frac{1}{2})} dy = \frac{1}{\sqrt{2}\pi^{\frac{1}{4}}} (2\varepsilon^2 \sqrt{\frac{1}{(\varepsilon^2 + \frac{1}{2})^3}} - \sqrt{\frac{1}{\varepsilon^2 + \frac{1}{2}}}). \tag{50b}$$

Equations (44), (48) and (49) show that the nonlinear interaction coefficients $N_1^{2,3}, N_2^{3,1}, N_3^{1,2}$ are purely imaginary numbers and are explicit functions of the frequency and wavenumber of the atmospheric Rossby wave (ω_2, k_2). In addition, as the triad interaction considered is due to the parameterized mass and momentum forcings, its dynamics should differ from the resonant triads arising from advective nonlinearity. However, in the specific parameter regime where the model has stable solutions, the triad displays certain properties similar to those of the conservative resonant interactions associated with advective nonlinearity.

The nonlinear interactions through physical parameterizations in (47) allow for the coupling of waves that belong to different fluid flows (sub-systems) and have distinctive temporal and spatial scales. Precisely, the distinctive nature of the atmospheric and oceanic fluid flows prevents a direct resonant atmosphere-ocean coupling through advection. Therefore, (47) represents a simplified mechanism by which the resonant interaction illustrated in Fig. 2 might occur.

b. Parametric Interactions

To further understand the interactions, we first analyze the limiting case where the interaction coefficient of the oceanic Kelvin mode is zero. This is equivalent to considering either a linear parameterization for the wind stress ($C_{\mathrm{Mflx}} = 0$) or the limiting case of $\varepsilon \to 0$. In this case, the oceanic Kelvin mode acts as a catalyst mode, i.e., it allows the nonlinear interaction between the two atmospheric waves but its amplitude is unaffected by the two atmospheric wave modes. This type of resonant interaction is known as 'Parametric interaction', as the magnitude of the energy exchange between the other triad members depends on the initial amplitude of the catalyst mode. Under the parametric interaction described above, equations (47) now read:

$$\frac{d}{dt}Z_1 = N_1^{2,3} Z_2 Z_3. \tag{51a}$$

$$\frac{d}{dt}Z_2 = N_2^{1,3} Z_1 Z_3^*. \tag{51b}$$

$$\frac{d}{dt}Z_3 = 0. \tag{51c}$$

An interpretation for (51) is that the slow oceanic wave amplitude evolution is even slower compared to the atmospheric wave amplitude evolution. In other words, there is a wide scale separation between the evolution of the atmosphere and the ocean.

Furthermore, from (51) one can obtain an equation for each of the atmospheric wave amplitudes. Thus, for the atmospheric Kelvin wave, we have:

$$\frac{d^2}{dt^2}Z_1 + \Omega^2 Z_1 = 0, \tag{52}$$

where

$$\Omega^2 \equiv -N_1^{2,3} N_2^{1,3} = C_h^2 \left[|\Lambda|^2 (I_{000}^{\varepsilon 1 \varepsilon})^2 - |\Gamma|^2 (I_{200}^{\varepsilon 1 \varepsilon})^2 \right] |Z_3|^2 \tag{53}$$

As $I_{000}^{\varepsilon 1 \varepsilon}$ and $I_{200}^{\varepsilon 1 \varepsilon}$ are polynomials in ε; both of them in combination with Λ and Γ determine the character of the slow wave modulation. Fig. 3 displays Ω^2 as a function of the oceanic to atmospheric meridional decay ratio (ε) for $C_h = |Z_3| = 1$ and (ω_2, k_2) taken from the equatorial $n = 1$ Rossby wave depicted in Fig. 2. Thus, we note that for typical values of the ratio between oceanic and atmospheric equatorial wave trappings $\varepsilon = \lambda_o/\lambda_a = \sqrt{U/C_a} \sim 0.2$ it follows that

$\Omega^2 > 0$ and, consequently, the atmospheric wave amplitudes undergo periodic modulation with frequency Ω. In contrast, for smaller values of ε (e.g. ~ 0.1) it results that $\Omega^2 < 0$ and the atmospheric wave amplitudes undergo an exponential growth, indicating an unstable character. In fact, Fig. 4 illustrates the integration of (51) for the unstable regime. A very fast exponential growth of the solutions at intraseasonal time-scales can be noted. Furthermore, as $\varepsilon = \lambda_o/\lambda_a$, it is suggested that the meridional trapping of the interacting equatorial waves is an important parameter to define the stability of the atmosphere-ocean resonant interactions.

In the parametric oscillatory regime of (51) i.e., $\Omega^2 > 0$, the total triad energy is bound and the oceanic wave amplitude is not modulated at the slow time scale. However, the oceanic wave is essential to allow the energy exchange between the atmospheric waves. The long period of energy exchange depends on the initial energy with which the triad was established. Thus, whenever $Z_3(t=0) \to 0$ then $\Omega \to 0$, and the modulation period becomes infinite. On the other hand, large values of $Z_3(t=0)$ result in large values of Ω, and, consequently, short periods for the energy exchange.

To further test the sensitivity of the system to the initial condition, i.e., the energy level at which the triad was established, Figs. 5 and 6 depict the integration of (51) for two different values of the initial oceanic wave amplitude, $|Z_3|^2 = 25$ and $|Z_3|^2 = 16$, respectively. In these numerical experiments $\varepsilon = \lambda_o/\lambda_a \sim 0.2$, and, therefore, the solution is stable (see Fig. 3). The selected initial energy distribution deposits more energy into the oceanic mode and less energy into the atmospheric Kelvin mode ($|Z_1|^2 = 0.32$). The atmospheric Rossby mode is initiated with an intermediate energy value ($|Z_2|^2 = 7.56$). From the time integration it can be seen that most of the energy goes to the atmospheric Kelvin mode, whereas the atmospheric $n = 1$ Rossby wave is modulated with the exact opposite phase. Thus, when the Rossby wave is at its maximum energy level, the atmospheric Kelvin wave is at its minimum energy level and *vice-versa*. Furthermore, as $|Z_3|^2$

decreases, the frequency modulation decreases, and the period of energy exchange increases from around 60 days to around 75 days. In both experiments, the energy of the oceanic Kelvin wave remains constant for the whole period.

c. Resonant Triad Interactions

We now analyze the dynamics of the same resonant triad discussed in the previous subsection, but considering a nonlinear wind stress parameterization ($C_{\mathrm{Mflx}} \neq 0$) or similarly relaxing the limiting case of $\varepsilon \to 0$ by considering ε small but finite. Although the coupling coefficient $N_3^{1,2}$ of the oceanic Kelvin mode must still be much smaller than those of the atmospheric members of the triad, now the amplitude of the oceanic mode is allowed to vary in time. Consequently, all the triad members undergo nonlinear amplitude modulation.

As in the parametric case, the full triad system (47) is integrable and its solutions are described in terms of Jacobi Elliptic functions (Abramowitz and Stegun 1972; Arfken and Weber 1995; Lynch 2003; Craik 1985). In this sense, to somewhat simplify the solution, we set the mode with the highest energy modulation (mode 1 - the atmospheric Kelvin mode) to have zero initial amplitude. In this case, the solution of system (47) is similar to that used by Domaracki and Loesch (1977); Raupp et al. (2008):

$$Z_1(t) = Z_2|_{t=0}\left(\left| \frac{N_1^{2,3}}{N_2^{1,3}} \right| \right)^{1/2} \mathrm{sn}(\Xi \,|\, \tilde{m}) \tag{54a}$$

$$Z_2(t) = Z_2|_{t=0}\, \mathrm{cn}(\Xi \,|\, \tilde{m}) \tag{54b}$$

$$Z_3(t) = Z_3|_{t=0}\, \mathrm{dn}(\Xi \,|\, \tilde{m}) \tag{54c}$$

where sn, cn and dn are the Jacobi elliptic functions, with argument Ξ (corresponding to the rescaled time) and parameter $\tilde{m}$ given by

$$\Xi = Z_3|_{(t=0)} \left(\left| N_1^{2,3} N_2^{1,3} \right| \right)^{1/2} \varepsilon t, \tag{55a}$$

$$\tilde{m} = \frac{N_3^{1,2} Z_2^2|_{(t=0)}}{N_2^{1,3} Z_3^2|_{(t=0)}}. \tag{55b}$$

The analytic solution (54) may exhibit different behaviors depending on the initial energy partition among the triad members. This is evidenced by the dependence of $\tilde{m}$ on the ratio of the initial amplitudes of modes 2 and 3. For example, when $\frac{Z_2^2|_{(t=0)}}{Z_3^2|_{(t=0)}} << 1$, the triad essentially undergoes the parametric regime discussed above, with mode 3 (the oceanic Kelvin mode) acting as a catalyst mode for the energy exchanges between the atmospheric waves. Moreover, when $\tilde{m} = 0$, the elliptic functions become trigonometric functions, with sn $\rightarrow$ sin, cn $\rightarrow$ cos and dn $\rightarrow +1$, resulting that $Z_3(t)$ is a constant. On the other hand, as the parameter $\tilde{m}$ tends to one, the elliptic functions describe a parabola, and instability of the highest frequency mode (mode 1) might occur. In addition, for intermediate values of the parameter $\tilde{m}$, the triad undergoes considerable energy exchanges, with all the wave amplitudes being significantly modulated in time. As the coupling coefficient of the oceanic mode is one order of magnitude smaller than those of the atmospheric waves, a sufficiently small initial amplitude of the oceanic Kelvin mode, in comparison with the atmospheric Rossby mode, is required in this regime.

A representative example of the solution (54) for the case of the full resonant triad interactions is illustrated in Fig. 7. The initial amplitudes for the modes 2 and 3 were chosen to fall into $0 < \tilde{m} < 1$ regime, and other parameters were set to yield $\varepsilon = 0.2$. As can be noted, all the triad members undergo significant interannual energy modulation. The dimensional natural oscillation periods associated with the triad members are: $T(\omega_1) = 3.4$ days, $T(\omega_2) = 12.0$ days and $T(\omega_3) = 57.0$ days. Therefore, the energy modulation of the triad members is much slower than their natural oscillation periods. Thus, the nonlinear triad interaction analyzed here allows for a multi time-scale interaction, yielding an interannual energy modulation through nonlinear interactions involving waves with synoptic and intraseasonal time-scales.

The resonant triad in Fig. 7 has a behavior typical of conservative resonant interactions through advective nonlinearity, that is, the highest absolute frequency mode of the triad (mode 1 - atmospheric Kelvin wave) always grows or declines at the expense of the other modes. Furthermore, the lowest absolute frequency mode of the triad (mode 3 - oceanic Kelvin mode) exhibits the weakest energy modulation. However, a difference between the present triad and a triad associated with advective nonlinearities is that the total energy of the present triad is no longer conserved. As a consequence, the total energy is also strongly modulated in the slow time scale. In addition, even though the atmospheric Kelvin wave is initiated with zero energy, this mode attains a much higher energy level than the remaining triad components, and, therefore, is responsible for almost all the energy of the system during the periods of its maximum energy level. These aspects are confirmed by the numerical integration of system (47), which agrees with the analytic solution (54) in all the correspondent parameter regimes.

In Fig. 8 the low-level patterns of the dynamical fields associated with the atmospheric branch of the resonant triad, i.e., the atmospheric Kelvin wave (mode 1) and the $n = 1$ equatorial Rossby wave (mode 2) are displayed. The Kelvin wave is of planetary scale and produces strong westerly winds throughout the Pacific Ocean (peaking over the central Pacific) and easterly winds outside the basin. In addition, the $n = 1$ equatorial Rossby (mode 2) produces a symmetric pattern about the equator, with strong westerlies both to the west and east of the Pacific basin and strong easterlies over the central Pacific. The spatial scale of the $n = 1$ Rossby wave is compatible with the pattern of twin cyclones around the eastern Indian Ocean, the Maritime continent and the western Pacific Ocean, that is associated to the MJO (e.g., Ferreira et al. (1996)).

The zonal wind stress produced by the interaction between modes 1 and 2 is displayed in Fig. 9. The strong wind stress over the western Pacific Ocean may represent the westerly wind burst that preceeds a typical El Niño development (see McPhaden (1999)). Over the eastern Pacific Ocean, the westerly wind stress is relatively weak, however, it can contribute to weaken the climatological trade winds and to relax the pressure gradient that maintains the warm waters to the west in the Pacific Ocean.

Furthermore, the coupling of the atmospheric Kelvin-Rossby waves and the oceanic Kelvin wave yields the modulated evaporation pattern depicted in Fig. 9. The evaporation envelope is about 6000 km of zonal extension (over the western Pacific), whereas its internal spatial structure is of synoptic or meso-γ spatial scale ($\approx$ 2000 km). The up and down synoptic-scale pattern of the evaporation may allow eastward propagation of the synoptic-scale convective anomalies that are part of the MJO envelope (see Zhang (2005)). Thus, the spatial patterns of the waves that constitute the resonant triad analyzed here are consistent with mechanisms that may lead to the interaction between synoptic, intraseasonal and interannual space/time scales.

Therefore, the results presented here for the special case of a single resonant triad interacting through parameterized atmosphere-ocean fluxes demonstrate the potential of the multiscale SInEN model to connect the atmosphere and ocean from synoptic to interannual time-scales through the intraseasonal time-scale.

6. Summary and Final Remarks

In this paper, we have developed a novel nonlinear multiscale model to study **S**ynoptic/**In**traseasonal/interannual-**E**l **N**iño (SInEN) interactions in a coupled atmosphere-ocean system. For this purpose, we have considered a simple set up, i.e., two coupled equatorial β-plane shallow-water equations, one representing the ocean and the other the atmosphere. The reduced multiscale SInEN model is obtained as a distinguished limit of the original coupled shallow-water equations. This limit represents a balanced regime in the atmosphere-ocean system where: the atmospheric Froude number; the oceanic Froude number; the non-dimensional strength of atmospheric height and oceanic thickness fluctuations, as well as the ratio between meridional and zonal length scales for both atmosphere and ocean, are all small parameters and of the same order of magnitude, that is:

$$\mathscr{F}_{r_a} = \mathscr{F}_{r_o} = F = \delta_a = \delta_o^{1/2} = \varepsilon. \tag{56}$$

This balance assumption is required for the mathematical consistence of the limiting dynamics and is physically coherent with the typical strengths for winds, currents and thermal anomalies associated with the scales centered around the intraseasonal variability. The selected equations (1) are compatible with the commonly adopted framework of applying shallow water equations to describe the first baroclinic mode of either the troposphere or the ocean active layer.

To bring about the SInEN regime, the mass and momentum forcings for the atmosphere and ocean are also expanded in terms of the small non-dimensional parameter of the system. The forcing strengths have been estimated in the context of the commonly held physical parameterizations for air-sea mass and momentum fluxes and deep convection in the atmosphere. For instance, the momentum forcing is represented through atmospheric wind stress, whereas the mass forcing is represented as the difference between evaporation (E) and deep convective precipitation (P). In turn, evaporation is formulated according to the wind induced surface heat exchange (WISHE) mechanism, while precipitation is formulated according to the wave-CISK hypothesis, where P is proportional to lower troposphere moisture convergence.

Although the flux formulation is recognized to be rather simplistic (Dijkstra 2000; Philander 1999b; Hirst and Lau 1990; Battisti 1988), some other drawbacks can be discussed. For example, in the SInEN model the atmosphere and ocean are not fully thermally coupled, since the impact of heat fluxes does not affect back the ocean thermodynamics and currents. The radiation-SST feedback and the evaporation feedback due to changing latent heat flux might also be considered. Further, the ocean thermohaline dynamics does not fully affect the ocean dynamics since $g' = \Delta\rho_o/\rho_o$ is constant, but in the real atmosphere-ocean system the exchanges of evaporation and precipitation along with the salinity also affect the density structure and play an important role in thermocline fluctuations. Furthermore, the ocean dynamics-thermodynamics coupling and the geometry of the Pacific Ocean are crucial for the formation of the warm/cold tongue during the El Niño/La Niña events, and thus it would be important to include these effects in our model along with the seasonal cycle.

The scalings used to obtain the SInEN model imply a referential intraseasonal time-scale connected to the fast equatorial synoptic and slow interannual time-scales through the non-dimensional parameter ε. Consequently, to obtain solutions of the SInEN equations, a perturbation theory with multiple time-scales has been adopted, with the atmospheric variables being assumed to evolve on the fastest two time-scales (synoptic and the referential intraseasonal), and the oceanic variables being assumed to evolve on the slowest two time-scales (the referential intraseasonal and the interannual). The leading order perturbations of each subsystem in the SInEN model are governed by the so-called equatorial β-plane linear long-wave equations, whose eigenvectors are the anisotropic non-dispersive Kelvin and Rossby waves.

These wave packets may undergo their own self-mode interactions through the intrinsic advective nonlinearity, and the parameterized mass and momentum fluxes can yield interactions between atmospheric and oceanic wave packets through resonant triads of specific Fourier modes. Therefore, our model might accommodate several dynamical mechanisms contained in other theoretical models, namely: the role of the intrinsic advective nonlinearity in the generation of low frequency variability (Ripa 1982, 1983a,b); the role of heating forcings in generating low-frequency variability by atmospheric only wave interactions (Raupp and Silva Dias 2009, 2010); the role of oceanic wave interactions with a diagnostic atmosphere in the excitation of El Niño (Battisti 1988); the role of interactions of linear modes through thermodynamics in the generation of low frequency variability in simple linear coupled ocean-atmosphere models (Hirst 1986; Hirst and Lau 1990), and the excitation of intraseasonal variability through atmospheric equatorial synoptic-scale turbulence (Biello and Majda 2005).

To illustrate the potential of the SInEn model to connect synoptic, intraseasonal and interannual time-scales in the atmosphere-ocean system, we have considered the special case of a single resonant triad involving an oceanic Kelvin wave, and an atmospheric Kelvin wave, and an atmospheric $n = 1$ Rossby wave, with the modes interacting resonantly through the parameterized atmosphere-ocean heat and momentum fluxes. The analytic solution of the triad equations shows that the oceanic wave may act as a catalyst mode for the energy exchanges between the atmospheric waves for linearized momentum flux. The oceanic Kelvin wave can also undergo significant energy modulations for a small but non-zero interaction coefficient, provided that this mode has a sufficiently smaller initial amplitude than the atmospheric waves. The results also show that the atmospheric Kelvin mode always supplies/receives energy to/from the remaining two triad components. In this situation, the wave amplitude modulations occur at interannual time-scales, while the phase propagation periods of the wave fields are of synoptic and intraseasonal time-scales.

Furthermore, the low-level spatial patterns of the triad members reinforce the potential of the resonant wave interaction mechanism through atmosphere-ocean coupling fluxes to connect synoptic, intraseasonal and interannual variabilities. In fact, for the atmospheric branch of the resonant triad, the low-level winds over the Pacific Ocean due to Kelvin wave activity are superimposed on the pattern produced by the $n = 1$ Rossby wave activity. The phases displayed for the atmospheric waves are in agreement with what is required by the amplitude modulation. Over the Pacific

Ocean, strong westerlies are found over both the western and eastern sides of the basin, whereas moderate winds are in the central Pacific. Associated to the wind patterns, planetary scale wind stress patches are found (~ 5000 km, see Fig. 9), and their tropical nature, magnitude and spatial scale suggest that they can be associated to the MJO. In addition, the nonlinear coupling to the ocean produces a synoptic scale structure for the evaporation field (~ 2000 km) that is modulated at planetary scales (~ 6000 km; see Fig. 9). The up and down synoptic scale pattern of the evaporation field may stimulate further eastward propagation of the intraseasonal activity and trigger oceanic Kelvin waves. Over the eastern Pacific Ocean, a relatively weak wind stress patch is found, which is associated to westerlies and thus tends to weaken the climatological trade winds and to reduce the east-west pressure gradient that maintains warm water to the west over the Pacific Ocean.

The next step to investigate the potential of the SInEn model in a more realistic scenario should be to restore the advective nonlinearities of each subsystem. The advection may couple each of the individual Fourier harmonics of the resonant triad analyzed here with all the wavenumbers of their corresponding wave packets. In fact, the model is weakly nonlinear in the ocean, but is fully nonlinear in the atmosphere.

Moreover, in the atmosphere, prognostic equations for the moisture field and interaction between different vertical modes should be considered in order to properly represent the cloud-radiation-SST feedback, as well as the intensification of the MJO through vertical tilting of the heating (a crucial aspect in multiscale models for the MJO e.g., Biello and Majda 2005; Thual and Majda 2016 and references therein). The variability of the solar radiative forcing may act as another forcing mechanism to enhance low-frequency atmospheric variability. Recently, by including linearized versions of some of the physical mechanisms described above, the reproduction of certain observed features of the MJO has been achieved (Majda and Stechmann 2009; Liu and Wang

2013). In principle, we believe that the theory constructed here can be generalized to include some of those more complex parameterizations described above, as far as the linear eigenvectors may still constitute the leading-order solutions in the new scenarios.

Thus, despite the aforementioned limitations, the advantage of the SInEn model is that it can be solved analytically, while keeping wave solutions in both the atmosphere and ocean. The SInEn model suggests that the resonant atmosphere-ocean coupling can be a possible mechanism for the generation of low frequency variability in the climate system. The various mechanisms involved, which determine the conditions for the establishment of the atmosphere-ocean resonant coupling, can be viewed as selection rules for the excitation of intraseasonal variability like in the MJO or even slower variability like the interannual El Niño variability.

Acknowledgments. Enver Ramirez wishes to thank to the São Paulo State Research Foundation (FAPESP) for his support under grant FAPESP 2006/60488-3. The work of Carlos Raupp was supported by FAPESP through grant 2009/11643-4. Pedro L. Silva Dias received support from the Brazilian National Research Council (CNPq) in Brazil, under two separate grants: 309395/2013-5 "Tropical Atmospheric Dynamics: Theory and Application" and the National Institute for Science and Technology for Climate Change (INCT)/CNPq National Institute for Science and Technology for Climate Change. This research was also funded by the Coordination for the Improvement of University Personnel (CAPES) Project PALEOCENE, IBM under the Open Source Cooperation Agreement No. B1258534, FAPESP grant PACMEDY Proj. No. 2015/50686 and the JPI Belmont PACMEDY project. This paper is dedicated to my family, special mention to my wife Rosio; her support during the long working hours and effort in reading and improving several versions of the manuscript was priceless, to Diego, Andrea, Guillermo, Susana, Nadia and Efrain, who have been a true source of motivation and are in the warmest place of my heart.

APPENDIX

Integrals involving Hermite functions

The evaluation of the product of modes requires the evaluation of integrals involving three or more Hermite functions. For the product of modes of the ocean and atmosphere, the meridional decays are different. The ocean is meridionally more confined than the atmosphere. In the ocean the Hermite functions are given by $\psi(y)$; whereas in the atmosphere they are given by $\psi(\varepsilon y)$ where ε is a measure of the meridional confinement. The Hermite functions ψ_m are related to the Hermite polynomials H_m by:

$$\psi_m(y) = \frac{\mathrm{e}^{-y^2/2}}{\sqrt{2^m m! \pi^{1/2}}} H_m(y); \tag{A1}$$

where $H_m(\xi) = (-1)^m \mathrm{e}^{\xi^2} \frac{\partial^m \mathrm{e}^{-\xi^2}}{\partial \xi^m}$. The meridional integration of the product of three Hermite functions with m,n and p nodes and different decays can be expressed by: $I^a_{mnp} = \int_{-\infty}^{+\infty} \mathrm{e}^{-y^2/a} H_m(\delta_m y) H_n(\delta_n y) H_p(\delta_p y)\, dy$. A practical rule to evaluate three or more Hermite functions is to reduce the functions in pairs until just one Hermite function remains, and then use the parity condition

$$I^a_m = \int_{-\infty}^{+\infty} \mathrm{e}^{-y^2/a} H_m(y)\, dy = \begin{cases} a^{1/2} 2^m \Gamma(\frac{m+1}{2})(a-1)^{m/2} & : m \text{ pair} \\ 0 & : m \text{ odd} \end{cases} \tag{A2}$$

a. Reduction in pairs for same meridional decays

In the simplest case of same meridional decays for the Hermite functions, the reduction in pairs is given according to Lord (1948); Busbridge (1948)

$$H_m(y)H_n(y) = m!n! \sum_{t=0}^{\min(m,n)} \frac{2^t}{t!(m-t)!(n-t)!} H_{m+n-2t}(y). \tag{A3}$$

Recursive application of the Busbridge identity (A3) and the parity condition (A2) allows the computation of the turbulent fluxes yielding slow time-scale modulation.

b. Reduction in pairs for different meridional decays

The general case of different meridional decays can also be performed by reduction in pairs. However, the decaying parameter enters in the product, and the results depend on the decaying parameter. Let $H_n(x)$ and $H_m(y)$ represent two Hermite polynomials with different meridional decays:

$$H_n(x)H_m(y) = \sum_{s,t=0}^{[m/2],[n/2]} \frac{(-1)^{s+t}(2x)^{n-2s}(2y)^{m-2t} n!m!}{(n-2s)!s!(m-2t)!t!}, \tag{A4}$$

where $[m/2]$ and $[n/2]$ represents the lowest nearest integer number, also known as the floor of the division $m/2$ and $n/2$, respectively. The order of the resulting polynomial is $n+m$, however, their coefficients depend on the decaying parameter.

Thus, for $x \to x$, $y \to \varepsilon x$, $n = 2$ and $m = 3$ we have

$$H_2(x)H_3(\varepsilon x) = 32\varepsilon^3 x^5 - (48\varepsilon + 16\varepsilon^3)x^3 + 24\varepsilon x \tag{A5}$$

For $x \to \varepsilon x$, $y \to x$, $n = 2$ and $m = 3$

$$H_2(\varepsilon x)H_3(x) = 32\varepsilon^2 x^5 - (24\varepsilon^2 + 16)x^3 + 24x \tag{A6}$$

Both results contrast with the simplest case of $x = y$, $n = 2$ and $m = 3$

$$H_2(x)H_3(x) = 32x^5 - 64x^3 + 24x \tag{A7}$$

Thus, the evaluation of the meridional integrals will depend on both the latitudinal structure of the involved modes and on their the meridional decays.

References

Abramowitz, M., and I. Stegun, 1972: *Parabolic Cylinder Functions*. U.S. Department of Commerce, National Bureau of Standards, Applied Mathematics Series, 55.

Arfken, G., and H. Weber, 1995: *Mathematical methods for Physicists*. Academic Press.

Battisti, D., 1988: Dynamics and Thermodynamics of a Warming Event in a Coupled Tropical Atmosphere-Ocean Model. *Journal of the Atmospheric Sciences*, pp. 2889–2919.

Biello, J. A., and A. J. Majda, 2005: A New Multiscale Model for the Madden-Julian Oscillation. *Journal of the Atmospheric Science*, **62**, 1694–1721.

Bony, S., and Coauthors, 2015: Clouds, circulation and climate sensitivity. *Nature Geoscience*, 261–268, doi:10.1038/ngeo2398.

Boyd, J., 1980: The nonlinear equatorial Kelvin wave. *Journal of Physical Oceanography*, pp. 1–11.

Busbridge, I. W., 1948: Some integrals involving hermite polynomials. *J. London Math. Soc*, **23**, 135–141.

Cane, M., and E. Sarachik, 1976: Forced baroclinic ocean motions I: The linear equatorial unbounded case. *Journal of Marine Research*, 629–665.

Craik, A., 1985: *Wave interactions and fluid flows*. Cambridge monographs on mechanics and applied mathematics.

Dijkstra, H., 2000: *Nonlinear Physical Oceanography: A Dynamical systems approach to the large scale ocean circulation and El Niño*. Kluwer Academic Publishers.

Domaracki, A., and A. Z. Loesch, 1977: Nonlinear interactions among equatorial waves. *Journal of the Atmospheric Science*, 486–498.

Donguy, J., and G. Meyers, 1987: Observed and modelled topography of the 20C isotherm in the tropical Pacific. *Oceanologica acta*, 41–48.

Emanuel, K., 1987: An air-sea interaction model of Intraseasonal Oscillations in the tropics. *Journal of the Atmospheric Science*, **44**, 2324–2340.

Ferreira, R., W. Schubert, and J. Hack, 1996: Dynamical aspects of twin tropical cyclones associated with the Madden-Julian oscillation. *Journal of The Atmospheric Sciences*, 929–945.

Fritz, S., 1958: Seasonal heat storage in the ocean an heting of atmosphere. *Arch Meteor Geophis Bio-klim*, 291–300.

Gabites, J., 1950: Seasonal variations in the atmospheric heat balance. Sc. d. thesis, Massachusetts Institute of Technonlogy, Massachusetts.

Gill, A., 1980: Some simple solutions for heat-induced tropical circulation. *Quarterly Journal of the Royal Meteorological Society*, 447–462.

Gill, A., 1982: *Atmosphere-Ocean Dynamics*. Academic Press.

Gill, A., and P. Phlips, 1986: Nonlinear effects on heat-induced circulation of the tropical atmosphere. *Quarterly Journal of the Royal Meteorological Society*, 69–91.

Hirst, A., 1986: Unstable and damped equatorial modes in simple coupled ocean-atmosphere models. *Journal of the atmospheric sciences*, 606–630.

Hirst, A., and K.-M. Lau, 1990: Intraseasonal and Interannual Oscillations in Coupled Ocean-Atmosphere Models. *Journal of Climate*, 713–725.

Holm, D. D., and P. Lynch, 2002: Stepwise precession of the resonant swinging-spring. *SIAM Journal of Applied Dynamical System*, 44–64.

Holton, J. R., 2004: *An introduction to dynamic meteorology, fourth edition*. Elsevier academic press.

Innes, P., 2002: Representation of the Madden-Julian oscillations in general circulation models. Ph.d. thesis, The university of Reading, Reading.

Inness, P., J. Slingo, S. Woolnough, R. Neale, and V. Pope, 2001: Organization of tropical convection in a GCM with varying vertical resolution: Implications for the simulation of the Madden-Julian Oscillation. *Climate Dynamics*, 777–793.

Johnson, R., T. Rickenbach, S. Rutledge, P. Ciesielski, and W. Schubert, 1999: Trimodal characteristics of tropical convection. *Journal of Climate*, 2397–2418.

Kevorkian, J., and J. Cole, 1986: *Multiple Scale and Singular Perturbation Methods*. Springer-Verlag New York, Inc.

Klein, R., and A. Majda, 2006: Systematic multiscale models for deep convection on mesoscales. *Theoretical Computational Fluid Dynamics*, **20**, 525–551, doi:10.1007/s00162-006-0027-9.

Krishnamurti, T., H. Bedi, and V. Hardiker, 1998: *Physical Processes*. Oxford University Press.

Liu, F., and B. Wang, 2013: An air-sea coupled skeleton model for the Madden-Julian oscillation. *Journal of Atmospheric Sciences*, 3147–3156.

Longuet-Higgins, M., and A. Gill, 1967: Resonant Interactions between Planetary Waves. *Proceedings of the Royal Society of London. Series A, Mathematical and Physical Sciences*, 120–144.

Lord, R. D., 1948: Some integrals involving hermite polynomials. *J. London Math. Soc*, **24 (2)**, 101–112.

Lynch, P., 2003: Resonant Rossby wave triads and the Swinging Spring - Supplement. *Bull. Amer. Meteor. Soc.*, 26–40.

Majda, A., 2002: *Introduction to PDE's and Waves for the Atmosphere and Ocean, Courant Lectures Note, 2002*. American Mathematical Society and Courant Institute of Mathematical Sciences.

Majda, A. J., and J. Biello, 2003: The Nonlinear Interaction of Barotropic and Equatorial Baroclinic Rossby Waves. *Journal of the Atmospheric Science*, **60**, 1809–1821.

Majda, A. J., and R. Klein, 2003: Systematic multiscale models for the Tropics. *Journal of the Atmospheric Science*, **60**, 393–408.

Majda, A. J., R. Rosales, E. Tabak, and T. C.V., 1999: Interaction of Large-Scale Equatorial Waves and Dispersion of Kelvin Waves through Topographic Resonances. *Journal of the Atmospheric Science*, **56**, 4118–4133.

Majda, A. J., and M. Shefter, 2001a: Models for Stratiform Instability and Convectively Coupled Waves. *Journal of the Atmospheric Science*, **58**, 1567–1584.

Majda, A. J., and M. Shefter, 2001b: Waves and Instabilities for Model Tropical Convective Parametrizations. *Journal of the Atmospheric Science*, **58**, 896–914.

Majda, A. J., and S. Stechmann, 2009: The skeleton of tropical intraseasonal oscillations. *Proc. Natl. Acad. Sci.*, **106**, 8417–8422.

McPhaden, M., 1999: Genesis and Evolution of the 1997-98 El Niño. *scie*, **12**, 950–954.

Menzaque, F., R. Rosales, E. Tabak, and C. Turner, 2001: The forced inviscid Burgers equation as a model for non-linear interactions among dispersive waves. *Contemporary Mathematics*, **283**, 51–82.

Nakazawa, T., 1988: Tropical super clusters within intraseasonal variations over the western Pacific. *Journal of the Meteorological Society of Japan*, 823–838.

Neelin, J. D., and N. Zeng, 2000: A Quasi-Equilibrium Tropical Circulation Model-Formulation. *Journal of the Atmospheric Sciences*, 1741–1766.

Pedlosky, J., 1987: *Geophysical Fluid Dynamics*. Springer-Verlag, New York.

Philander, S. G., 1999a: *El Niño, La Niña and the Southern Oscillation, International Geophysical Series*. Academic Press.

Philander, S. G., 1999b: *El Niño, La Niña and the Southern Oscillation, International Geophysical Series*. Academic Press.

Ramírez, E., P. L. Silva Dias, and C. Raupp, 2011a: Asymptotic approach fot the nonlinear equatorial long wave interactions. *J. Phys.: Conf. Ser.*, **285**, 012 020, doi:doi:10.1088/1742-6596/285/1/012020.

Ramírez, E., P. L. Silva Dias, C. Raupp, and J. P. Bonatti, 2011b: The family of anisotropically scaled equatorial waves. *Journal of advances in modeling earth systems*, **3**, 000–000.

Raupp, C. F. M., and P. L. Silva Dias, 2005: Excitation Mechanism of Mixed Rossby-Gravity Waves in the Equatorial Atmosphere: Role of the Nonlinear Interactions among Equatorial Waves. *Journal of Atmospheric Sciences*, **62**, 1446–1462.

Raupp, C. F. M., and P. L. Silva Dias, 2006: Dynamics of resonantly interacting equatorial waves. *Tellus Series A*, **58**, 263–279, doi:{10.1111/j.1600-0870.2006.00151.x}.

Raupp, C. F. M., and P. L. Silva Dias, 2009: Resonant wave interactions in the presence of a diurnally varying heat source. *Journal of the Atmospheric Sciences*, **66**, 3165–3183.

Raupp, C. F. M., and P. L. Silva Dias, 2010: Interaction of equatorial waves through resonace with the diurnal cyle of tropical heating. *Tellus*, **62A**, 706–718.

Raupp, C. F. M., P. L. Silva Dias, P. Milewski, and E. Tabak, 2008: Resonant wave interactions in the equatorial waveguide. *Journal of the Atmospheric Sciences*, **65**, 3398–3418.

Reed, R., and E. E. Recker, 1971: Structure and Properties of Synoptic-Scale wave disturbances in the equatorial western Pacific. *JAS*, **28**, 1117–1133.

Ripa, P., 1982: Nonlinear Wave-Wave Interactions in a One-Layer Reduced-Gravity Model on the Equatorial β Plane. *Journal of Physical Oceanography*, **12**, 97–111.

Ripa, P., 1983a: Weak Interactions of Equatorial Waves in a One-Layer Model. Part I: General Properties. *Journal of Physical Oceanography*, **13**, 1208–1226.

Ripa, P., 1983b: Weak Interactions of Equatorial Waves in a One-Layer Model. Part II: Applications. *Journal of Physical Oceanography*, **13**, 1227–1240.

Rogers, R., 1976: *Water vapor and its thermodynamic effets*. Pergamon Press.

Schubert, W., L. Silvers, M. Masarik, and A. Gonzalez, 2009: A filtered model of tropical wave motions. *Journal of Adv. Mod. exEarth Syst.*, **1**, 1–11.

Stevens, B., and S. Bony, 2013: What are climate models missing. *Science*, **340**, doi:10.1126/science.1237554.

Suarez, M., and P. Schopf, 1988: A Delayed Action Oscillator for ENSO. *jas*, **45**, 3283–3287.

Thual, S., and A. J. Majda, 2016: A skeleton model for the MJO with refined vertical structure. *Climate Dynamics*, doi:10.1007/s00382-015-2731-x.

Torrence, C., and P. Webster, 1999: Interdecadal changes in the ENSO-Monsoon System. *Journal of Climate*, 2679–2690.

Wang, C., and R. Weisberg, 1994: Equatorial trapped waves of a coupled ocean-atmosphere system. *Journal of Physical Oceanography*, **24**, 1978–1998.

Yano, J.-I., M. J.C., and M. M.W., 1995: Hierarchical Tropical cloud systems in an analog shallow-water model. *Journal of the Atmospheric Science*, **52**, 1723–1742.

Zdunkowski, C., and A. Bott, 1980: *Dynamics of the atmosphere: A course in theoretical meteorolgy*. University Press of Florida.

Zebiak, S., 1982: A simple atmospheric model of relevance to El Niño. *Journal of the Atmospheric Science*, **39**, 2017–2027.

Zebiak, S., and M. Cane, 1987: A Model El Niño Southern Oscillation. *Monthly Weather Review*, 2262–2278.

Zhang, C., 2005: Madden-Julian oscillation. *Review of Geophysics*, doi:10.1029/2004RG000158.

LIST OF TABLES

TABLE 1. Typical values of the model parameters

Symbol	Value	Parameter
ε	0.1	scale separation factor
H_a	250 m	atmosphere equivalent depth
H_o	150 m	ocean equivalent depth
h_b=εH_a	25 m	boundary layer depth
l_s	15×10^6 m	zonal length scale of the Pacific Ocean
λ_a	15×10^5 m	atmospheric deformation radius
λ_o	4×10^5 m	oceanic deformation radius
F	0.1	height fluctuation allowed
$C_{a_{ref}}=C_a$	50 m s^{-1}	atmospheric gravity wave speed of the first baroclinic mode
$v_{a_{ref}}=u_a$	5.5 m s^{-1}	referential speed for slower wave modes
$C_{o_{ref}}=C_o$	2.5 m s^{-1}	oceanic gravity wave speed of the first baroclinic mode
$U=(v_{a_{ref}}+C_{o_{ref}})/2$	4.9 m s^{-1}	referential speed for the SInEN regime
ρ_a	1.1 kg m^{-3}	air density
ρ_o	1.0×10^3 kg m^{-3}	water density
N	10^{-2} s^{-1}	Brunt-Vaisala frequency
q_r	12 g kg^{-1}	referential moisture
$\bar{T}$	301 K	mean temperature
T_0	273.0 K	referential temperature
λ_p	0.9	precipitation efficiency
β	2.29×10^{-11} m^{-1}s^{-1}	Coriolis meridional gradient
L_v	2.50×10^6 J kg^{-1}	vaporization latent heat
R_v	461.50 J kg^{-1}K^{-1}	moist air gas constant
R_d	287.04 J kg^{-1}K^{-1}	dry air gassy constant
g	9.8 m s^{-2}	vertical acceleration due to gravity
g'	5.6×10^{-2} m s^{-2}	reduced gravity
e_{s_0}	6.11 mb	saturation vapor pressure at T_0
C_d	1.1×10^{-3}	drag coefficient

LIST OF FIGURES

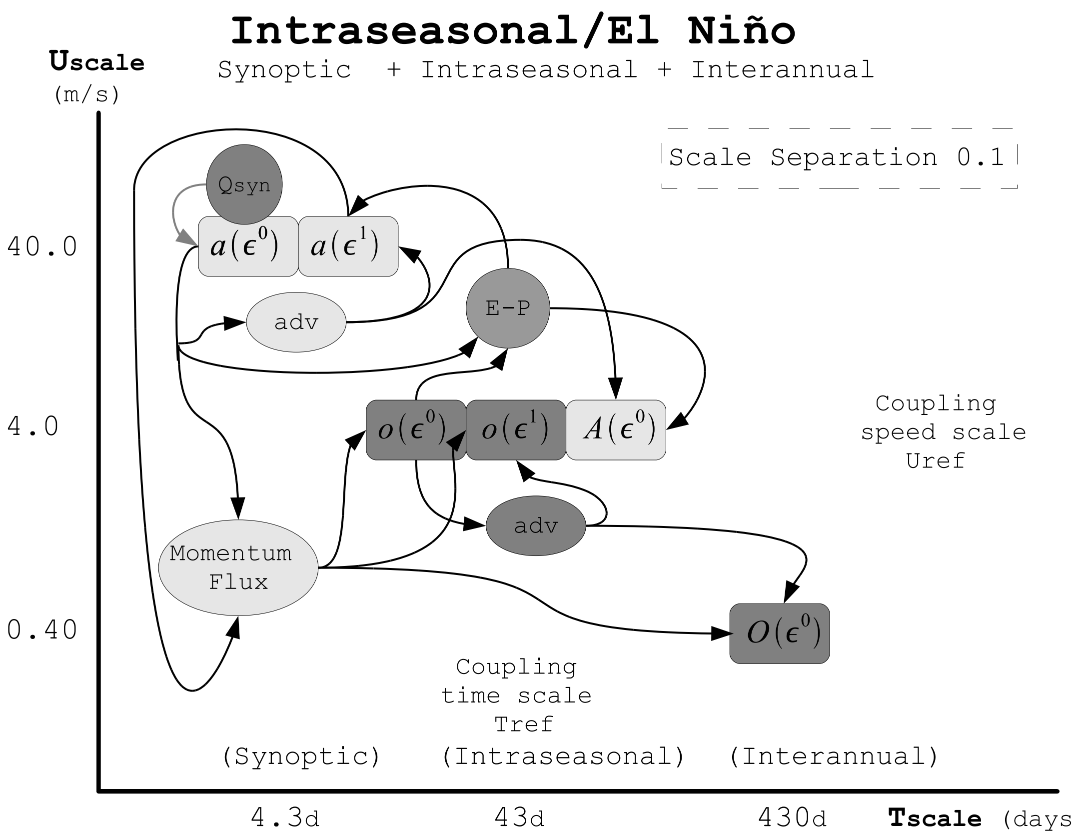

FIG. 1. Schematic diagram for the Synoptic/Intraseasonal/interannual-El Niño interactions (SInEN Regime). $A(\varepsilon^0)$ and $O(\varepsilon^0)$ represent the slowly variant atmospheric and ocean energies, respectively. Similarly, $a(\varepsilon^0)$ and $o(\varepsilon^0)$ are the leading order atmospheric, and ocean perturbations and $a(\varepsilon^1)$ and $o(\varepsilon^1)$ are higher order atmospheric and ocean perturbations. The term adv is the advective nonlinearity, E−P is the mass flux and $Q_{synoptic}$ is the external synoptic forcing. The scale separation in both the speed and time are given by $\varepsilon = 0.1$.

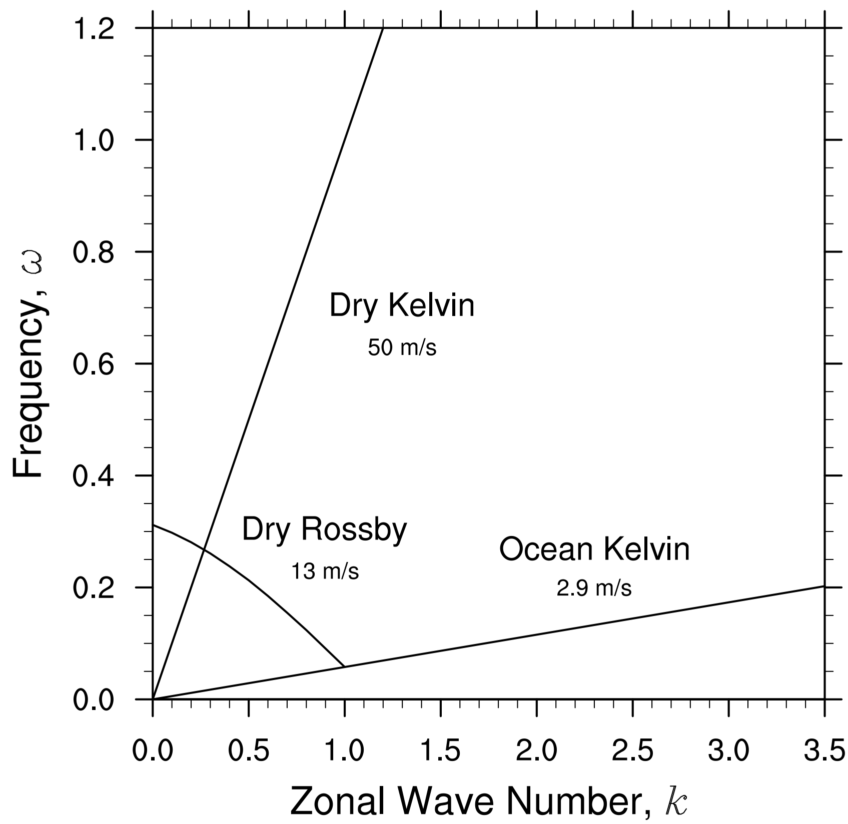

FIG. 2. Dispersion wavenumber-frequency diagram depicting the possibility of a resonant triad involving an atmospheric dry Kelvin wave; an atmospheric dry Rossby wave and an oceanic Kelvin wave. The term "dry" refers to the eigenfrequency of the equatorial wave mode not modified by coupling with deep convection. The wavenumbers/frequencies are non-dimensional, however, the dimensional phase speeds (m/s) of the corresponding waves are also displayed. To determine the resonant triad, the origin of the dispersion curve of the atmospheric Rossby wave is symmetrically displaced to a point over the oceanic Kelvin wave dispersion curve. Thus, the intersection between the dispersion curves of the atmospheric Kelvin and Rossby waves determines a set of three wave modes satisfying the resonance conditions (39).

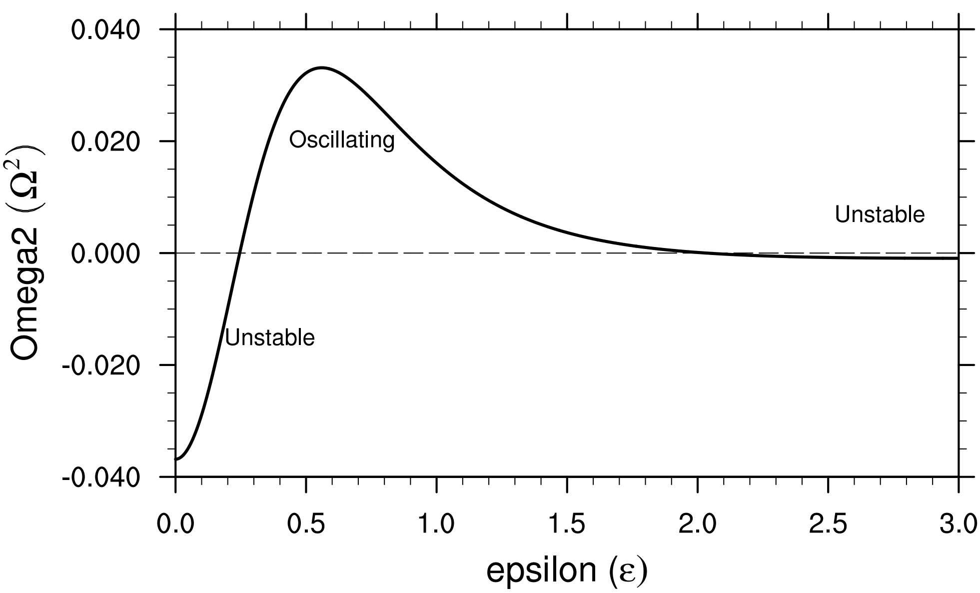

FIG. 3. Ω^2 as a function of the ocean to atmosphere meridional decay ratio $\left(\delta_o/\delta_a\right) = \varepsilon$ for $C_h = |Z_{oK}| = 1$.

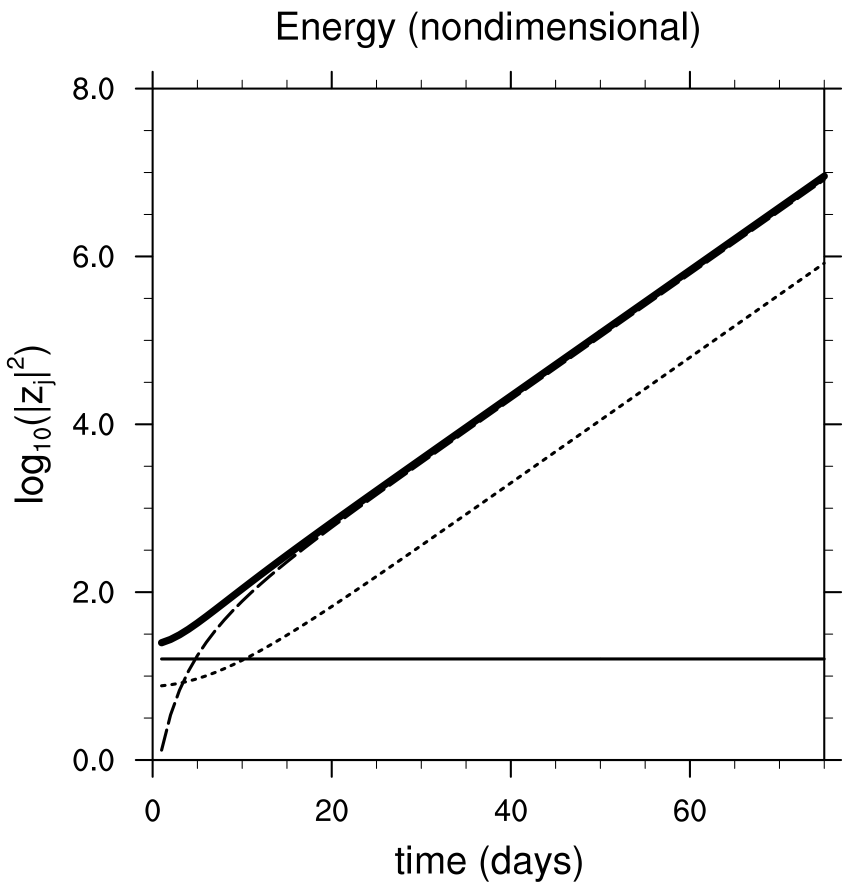

926 FIG. 4. Energy modulation of the resonant triad interaction illustrated in Fig 2 for the unstable regime depicted in Fig. 3. The thick line is the total energy, and the thin line is the energy of the oceanic wave, which remains bound. The dotted line is the energy of the atmospheric Rossby wave, and the long dashed line is the atmospheric Kelvin wave energy. The $\log_{10}$ of the energy scale indicates the exponential growth at an intraseasonal time-scale.

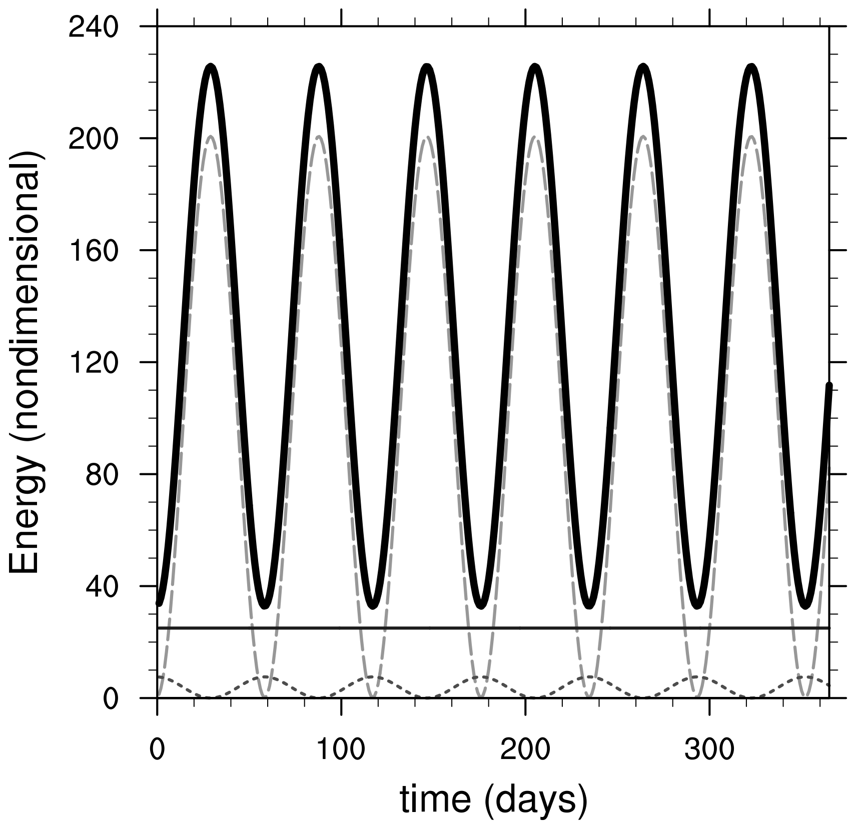

FIG. 5. Time evolution of the mode energies for the resonant triad interaction illustrated in Fig. 2 but for $\lambda_o/\lambda_a = 0.28$ (stable regime). The triad is composed of: an atmospheric Kelvin wave (mode 1 - long dashed line), an atmospheric $n = 1$ Rossby wave (mode 2 - short dashed line) and an oceanic Kelvin wave (mode 3 - thin continuous line). The total energy of the triad is also displayed (thick continuous line). The initial amplitudes of the modes are set to $|Z_1|^2 = 0.32, |Z_2|^2 = 7.56, |Z_3|^2 = 25$. Other parameters are set to $q_r = 1.49, C_u = C_{Pr} = 0, C_h = 11.0, C_{Mflx} = 0, \phi_1 = \pi/6, \phi_2 = 2\pi/6, \phi_3 = 0$.

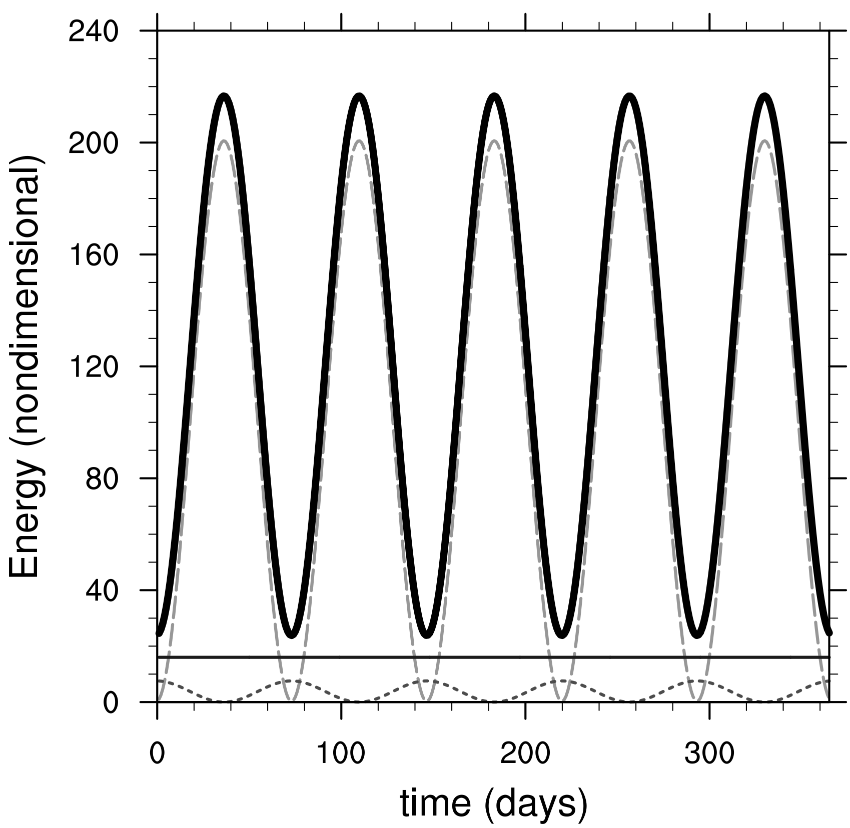

FIG. 6. Same as Fig. 5 but for $|Z_3|^2 = 16.0$.

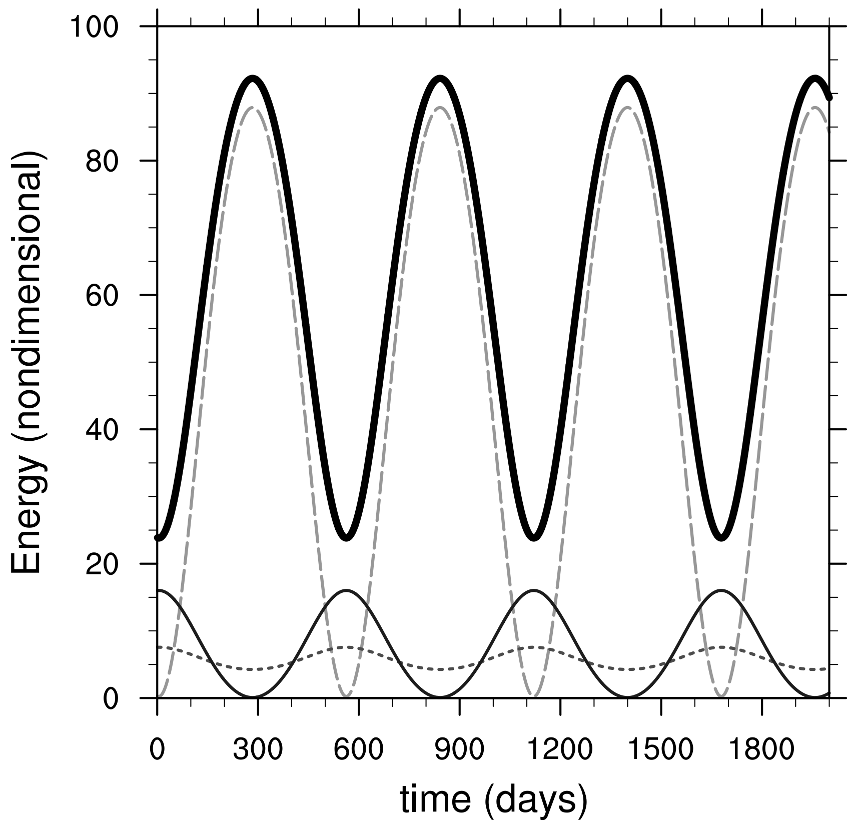

937 FIG. 7. Similar to Fig. 5 but for the general case where the wave amplitudes are governed by equation 47. The triad is made of: an atmospheric Kelvin mode (mode 1 - long dashed line), an atmospheric Rossby mode (mode 2 - short dashed line) and an oceanic Kelvin mode (mode 3 - continuous line). Total energy of the triad is also displayed (thick continuous line). The initial amplitudes are set as $|Z_3(0)|^2 = 25.0, |Z_2(0)|^2 = 7.56$ and $|Z_1(0)|^2 = 0.0$. The model parameter values considered in this integration are: $q_r = 1.49, C_u = 0.0, C_{Pr} = 0.0, C_h = 1.1$ and $C_{Mflx} = 1.0$.

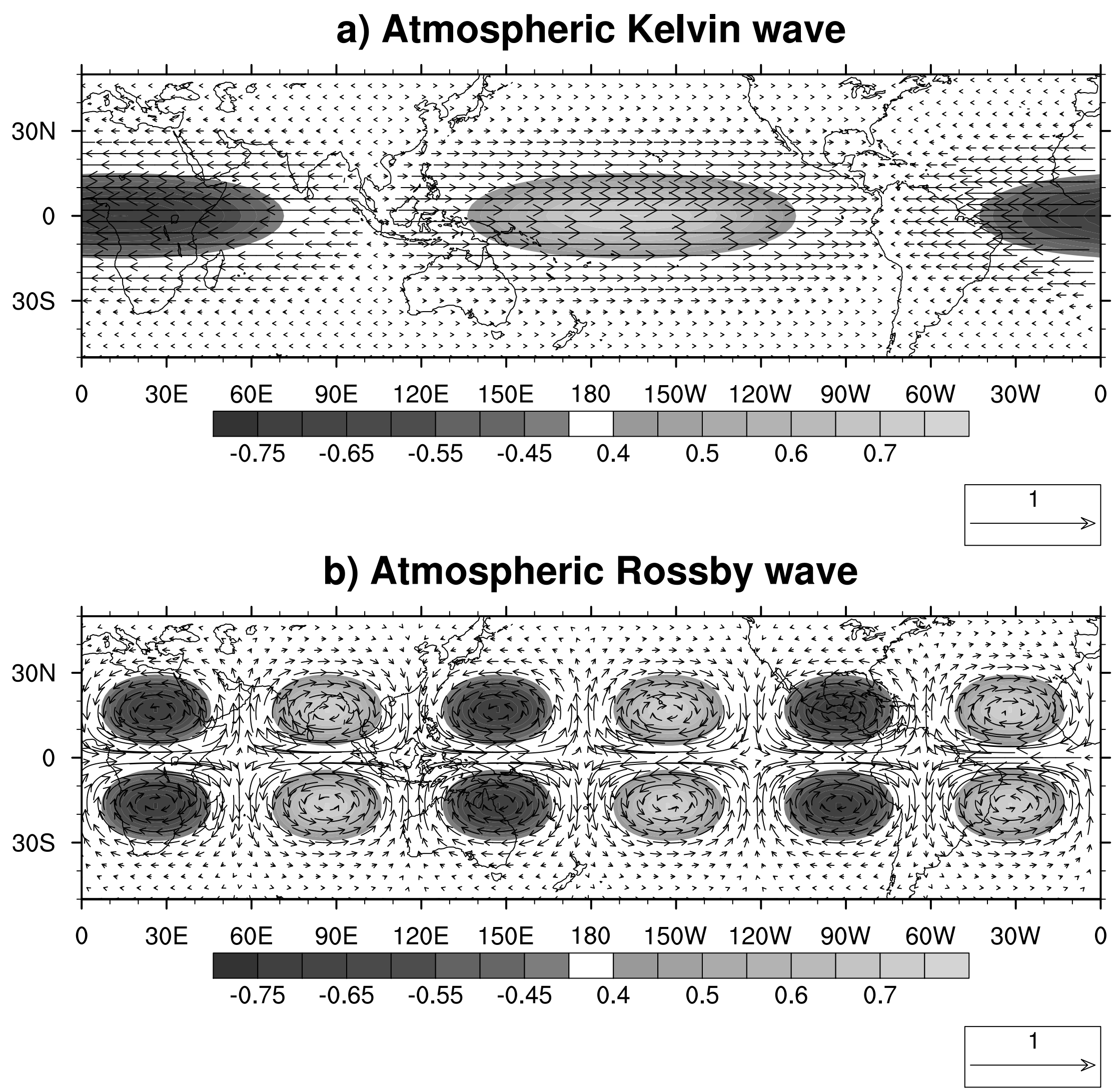

FIG. 8. Horizontal structure of the low-level horizontal wind and height fields for (a) the atmospheric first baroclinic equatorial Kelvin wave with the dimensionless zonal wavenumber $k_1^* = 0.27$ and frequency $\omega_1^* = 0.27$ and, (b) the atmospheric first baroclinic $n = 1$ equatorial Rossby wave, with dimensionless zonal wavenumber $k_2^* = 0.73$ and frequency $\omega_2^* = 0.21$. Both of these waves constitute the resonant triad illustrated in Figs. 5-7.

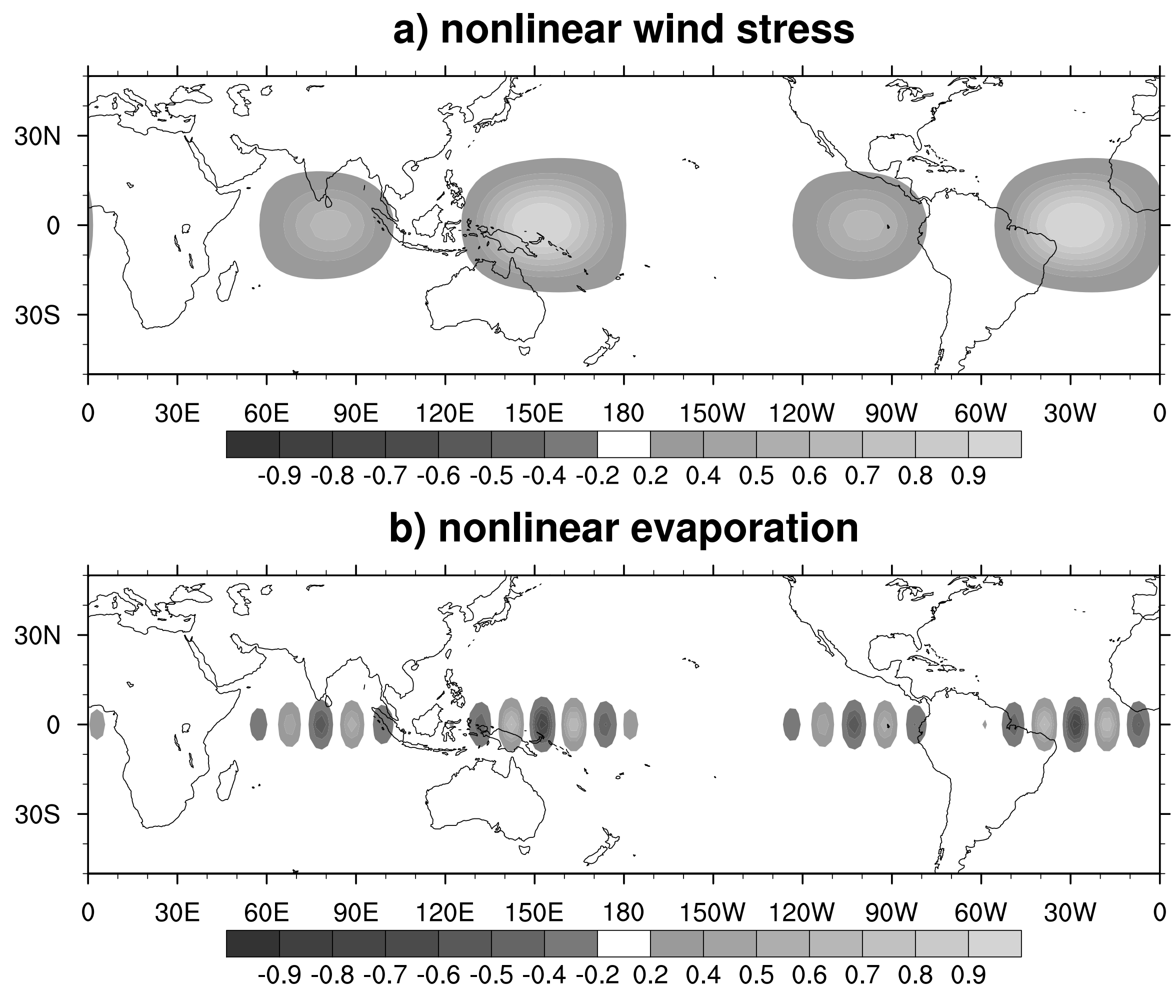

FIG. 9. (a) Zonal wind stress produced by the interaction of the atmospheric Kelvin wave and the $n = 1$ Rossby wave (Fig. 8a-b). Over the Pacific Ocean, the wind stress is associated with westerlies. The intense westerlies over the western Pacific Ocean may trigger the oceanic Kelvin wave propagation, which is important for onset of El Niño. Westerly winds over the western Pacific and Indian Oceans are sometimes associated to the MJO. Over the eastern Pacific, low-level westerlies may lead to the weakening of the trade winds and relax the pressure gradient that maintains warm waters and deep convection to the west of the Pacific Ocean; (b) spatial pattern of the evaporation field produced by the coupling between the atmospheric Kelvin-Rossby waves and the oceanic Kelvin mode. The spatial modulation over the western Pacific is about 60 degrees ($\approx$ 6000 km), and an internal structure of synoptic or meso-γ scale ($\approx$ 2000 km) is noted. Over the western Pacific and Indian Ocean the internal structure may lead to the propagation of synoptic scale convection to the east along with the MJO signal. This configuration also reinforces the atmospheric configuration displayed in Fig. 8 and Fig. 9a.